Spectrochimica Acta. Vol. 44A, No. 2. pp. 185–208, 1988.
Printed in Great Britain.

0584–8539/88 $3.00 + 0.00
Pergamon Press plc

Vibrational analysis of cyclo(D-Ala-L-Ala) in two crystalline forms. Effect of structure on peptide group and CH modes*

T. C. CHEAM and S. KRIMM

Biophysics Research Division and Department of Physics, University of Michigan, Ann Arbor, MI 48109, U.S.A.

(*Received* 8 *May* 1987; *in final form* 27 *June* 1987; *accepted* 29 *June* 1987)

Abstract—Cyclo(D-Ala-L-Ala) has been found by X-ray diffraction to crystallize in two forms with different hydrogen bond patterns and strengths and different conformations of the $C^{\alpha}H^{\alpha}C^{\beta}H_3$ group. We have done a comprehensive analysis of the Raman and i.r. spectra of both forms and their N-deuterated derivatives. Spectra were taken of oriented single crystals, polycrystalline powders, and aqueous solutions, allowing a virtually complete vibrational assignment. Systematic, distinct differences were observed in the modes of the CONH group and in the CH stretching and bending modes. These spectral differences have been correlated with the different molecular and crystal structures. In particular, the width and sub-band structure of the NH stretch mode and the splittings of the CO stretch are shown to be related to the hydrogen bond pattern, and the NH bend modes are found to be relatively as sensitive to the hydrogen bond strength as is the NH stretch. The differences in the CH^{α} bend modes show that both conformations exist in solution. *Ab initio* molecular orbital calculations have been done to understand the frequency shifts of the NH and CH^{α} stretch modes in the two forms. Normal mode calculations were also done.

INTRODUCTION

We have previously described a comprehensive analysis of the Raman and i.r. spectra of cyclo(Gly-Gly) and five of its isotopic derivatives [1, 2]. In this paper we report on a study of the next simplest cyclic peptide, cyclo (D-Ala-L-Ala).

Besides further elucidating the modes characteristic of the *cis* peptide group, cyclo(D-Ala-L-Ala) is especially interesting in its own right. This compound has been found to crystallize in two forms with very different hydrogen bonding configurations (Fig. 1). In one, which we will designate as form **I** following SLETTEN [3], the molecules form hydrogen-bonded layers [4, 5], whereas in form **II** hydrogen-bonded chains similar to those in cyclo(Gly-Gly) are present [3]. In addition, the dimensions of each N–H · · · O=C group (Fig. 1) suggest that the hydrogen bonds in **II** are stronger than those in **I**. We will see that the different hydrogen bond patterns and strengths result in systematic differences in the spectra of the two forms, thus shedding light on the sensitivity of various modes to hydrogen bonding. We have recently studied by *ab initio* molecular orbital methods the changes in the harmonic force constant and i.r. intensity of the peptide NH stretch mode as a function of hydrogen bond geometry [6]. Similar calculations for the other peptide group modes would be much more difficult because these modes are more delocalized. Cyclo(D-Ala-L-Ala) provides a very convenient system where the effects of hydrogen bond geometry on these other modes, as well as on the NH stretch, can be studied experimentally. Though the peptide groups in cyclo (D-Ala-L-Ala) are in the *cis* conformation, our results should provide at least a qualitative guide in studying the modes of *trans* peptides.

Furthermore, the methyl side chains are more nearly axial in **I** than in **II**; conversely, the CH^{α} bond is more nearly axial in **II** (Fig. 1). We find distinct differences between **I** and **II** in the frequencies and intensities of the CH^{α} stretching and bending modes and the CH_3 antisymmetric stretches, suggesting a correlation of these modes with the conformation of the $CH^{\alpha}CH_3$ group.

Much less work has been done on cyclo(D-Ala-L-Ala) than on cyclo(Gly-Gly). BROCKMANN and MUSSO [7] recorded the i.r. spectrum of form **I**, and STEIN [8] measured i.r. and Raman spectra, also of **I**. Only a partial assignment was given by these workers. We will present the results of Raman and i.r. studies of **I** and **II** and their N-deuterated derivatives, and of normal mode calculations of the crystals. Our data and calculations have allowed a nearly complete vibrational assignment of cyclo(D-Ala-L-Ala), with tentative assignments only for the methyl torsion mode and for the far i.r. region. *Ab initio* calculations were also done to understand some of the observations.

EXPERIMENTAL

The cyclo(D-Ala-L-Ala) was synthesized by ANITA GO in Prof. K. D. KOPPLE's laboratory. Crystals were grown by slow evaporation from aqueous solution. Form **I** grows as chunky crystals at room temp., and form **II** as thin platelets at higher temperatures (we used 50–70°C). We found it easier to get form **II** than form **I**. The N-deuterated materials were obtained from D_2O solution, but we were unable to grow single crystals of **I**–ND. Single-crystal films for polarized i.r. studies were prepared by cleaving from thicker pieces.

Spectra were run with a Spex 1403/Datamate system with excitation from the 514.5 nm line of a Spectra Physics 165

*This is paper number 37 in a series, "Vibrational analysis of peptides, polypeptides, and proteins".

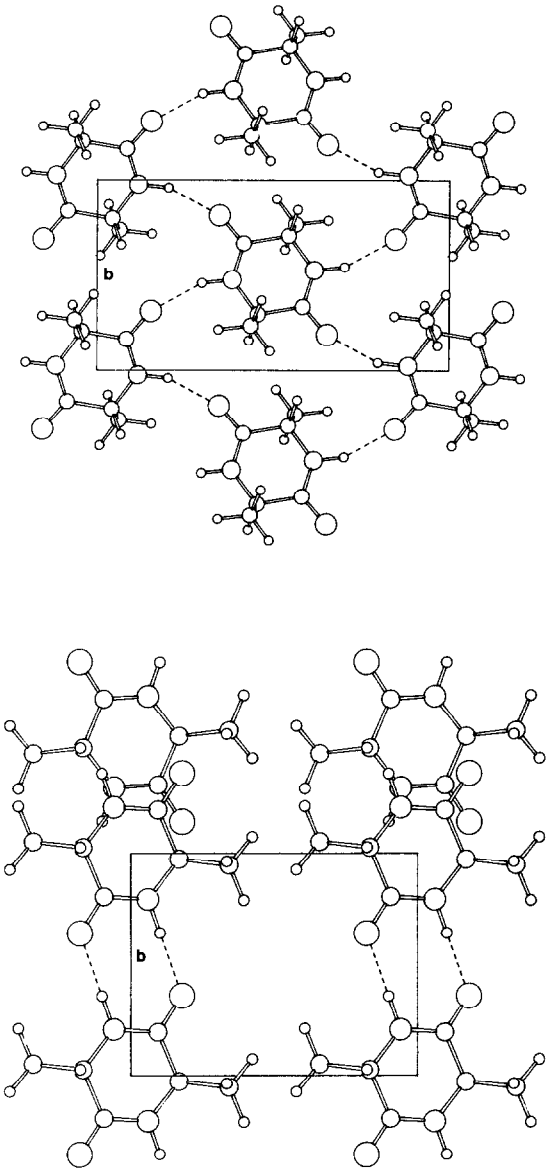

Fig. 1. Cyclo(D-Ala-L-Ala) crystal structures. Top: Form I, space group $P2_1/n$. Viewed perpendicular to (101). Hydrogen bond dimensions: R(N · · · O) = 2.866 Å, R(C=O) = 1.236 Å, θ(HNO) = 15.0°, θ(CON) = 146.0°. Bottom: Form II, space group $P2_1/c$. Viewed along c axis. Hydrogen bond dimensions: R(N · · · O) = 2.859 Å, R(C=O) = 1.241 Å, θ(HNO) = 3.6°, θ(CON) = 124.1°.

argon ion laser, and on a Bomem DA3 Fourier transform i.r. spectrometer. The bandpass in the Raman experiments on powders and single crystals was 1–2 cm^{-1} with laser powers of about 300 mW at the sample. The i.r. powder spectra were run at 1 cm^{-1} resolution in the 4000–400 cm^{-1} region and at 2–4 cm^{-1} below 400 cm^{-1}; the spectrometer was evacuated to less than 2 torr. Powder spectra at liquid nitrogen temperature were obtained using an Air Products LT-3-110 cryostat and homemade cells. I.r. spectra of powdered samples were run in KBr pellets and, below 300 cm^{-1}, as pressed films. For the Raman spectra, the powder was packed into glass capillaries. Solution spectra at room temperature were taken using standard i.r. liquid cells and glass capillaries.

The single-crystal spectra were run with (101) sections of **I** and with (100) sections of **II**, these faces being cleavage planes. Since both forms are monoclinic, the extinction directions in each specimen are along and perpendicular to b. The Cartesian axes and polarization directions used in our work are defined as follows. In **I**, y is parallel to b and z perpendicular to (101); in **II**, y is also parallel to b and z is along c. That is, in Fig. 1 the x, y, and z axes are oriented in the conventional manner in each structure: x horizontal, y vertical, and z out of the plane of the figure.

NORMAL MODE CALCULATIONS

The crystal structures of E. SLETTEN [5] and J. SLETTEN [3] were used. E. SLETTEN's X-ray determination of **I** seems more reliable than the study by BENEDETTI *et al.* [4]. As we did for cyclo(Gly-Gly), we modified the NH and CH bonds given by J. SLETTEN for **II** to 1.00 Å and 1.09 Å, respectively; we used similarly modified hydrogen atom positions given for **I** by E. SLETTEN.

The normal mode calculations were done in a Cartesian coordinate basis, and factoring of the secular equation for the crystals was based on KOBAYASHI's [9] method. Both crystal forms are monoclinic with two molecules per unit cell. In both forms the factor group is isomorphic to C_{2h} and four symmetry blocks result: A_g, B_g, A_u, and B_u, each of dimension 30×30 corresponding to the asymmetric unit ($CONHCHCH_3$).

The internal and local symmetry coordinates for the peptide group and alanyl residue are as given in [2] and [10], respectively. The intramolecular force field is a combination of the cyclo(Gly-Gly) set and the alkane field of [11]. The cyclo(Gly-Gly) force constants (Set II in [2]), which were refined in a non-redundant basis, were transformed into the local symmetry basis. The parameters relating to the peptide group were then transferred to cyclo(D-Ala-L-Ala). To this set were added force constants from [11] for the $CHCH_3$ group, except that the $C^{\alpha}C^{\beta}$ torsion force constant was taken from β-poly(L-alanine) [10] because of the different definition of the torsional coordinate used in [11].

While we eventually intend to refine a force field for cyclo(D-Ala-L-Ala), our present calculations were done mainly to help in assigning the spectra. We have therefore not tried to adjust the force constants to get better agreement with observed frequencies, except for the CH_3 stretch modes, which could be easily improved by modifying the diagonal CH force constant to 4.800 mdyne/Å (from 4.699) and the CH, CH interaction term to 0.050 mdyne/Å (from 0.043).

Intermolecular force constants were computed from the 6–12 atom–atom potential of MOMANY *et al.* [12] with a cut-off radius of 5 Å and without linear terms in the Cartesian derivatives [9]. We assumed values of 0.12 and 0.15 mdyne/Å for the hydrogen bond H · · · O interaction in **I** and **II**, respectively; the value for **II** is the same as for cyclo(Gly-Gly). On addition of the intermolecular terms, the deformation modes in-

volving the H^{α} and CH_3 groups shift considerably and generally become in worse agreement with the data. Because the alkane force field was refined without taking into account non-bonded interactions, and since the peptide group modes shift less, we will report only the intramolecular frequencies calculated without the atom–atom terms. The lattice modes given are calculated with the complete intramolecular and intermolecular force field.

SPECTRAL ASSIGNMENTS

Our Raman and i.r. room temp. spectra of cyclo (D-Ala-L-Ala) are shown in Figs 2–14. By comparison with spectra of less pure samples, bands due to impurities were identified in the N-deuterated materials. Table 1 lists the observed frequencies and their assignments. Table 2 gives the calculated frequencies of an isolated type **II** molecule (of C_i symmetry), and Table 3 shows the calculated lattice frequencies for the two crystal structures. For brevity, we list the calculated intramolecular modes for **II** and **II**–ND only; major differences in the results for **I** will be noted in the discussion. Figure 15 shows ORTEP plots of the atomic displacements for the intramolecular Raman-active modes of **II**, and Figs 16 and 17 show the lattice modes of **I** and **II**.

With 20 atoms in a centrosymmetric molecule, there are 27 intramolecular modes in each of the four symmetry species. There are 6 Raman-active rotatory

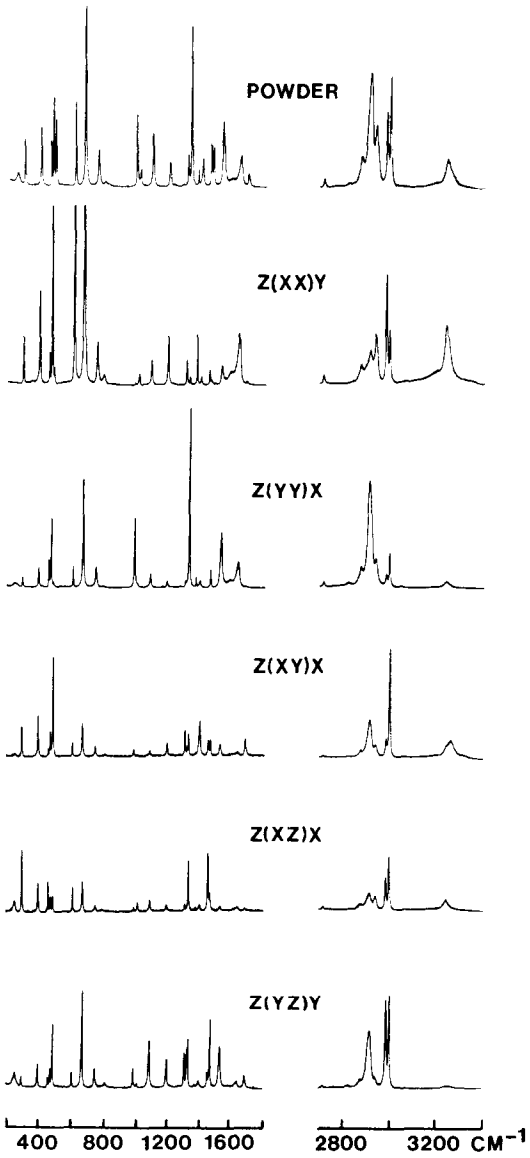

Fig. 2. Raman spectra of form **I** powder and single crystal.

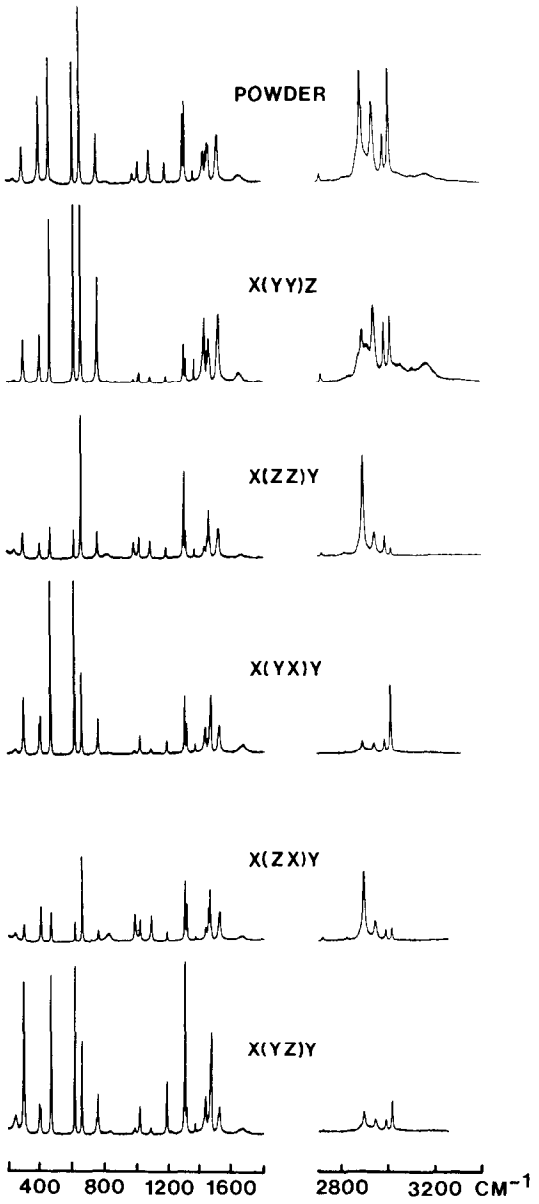

Fig. 3. Raman spectra of form **II** powder and single crystal.

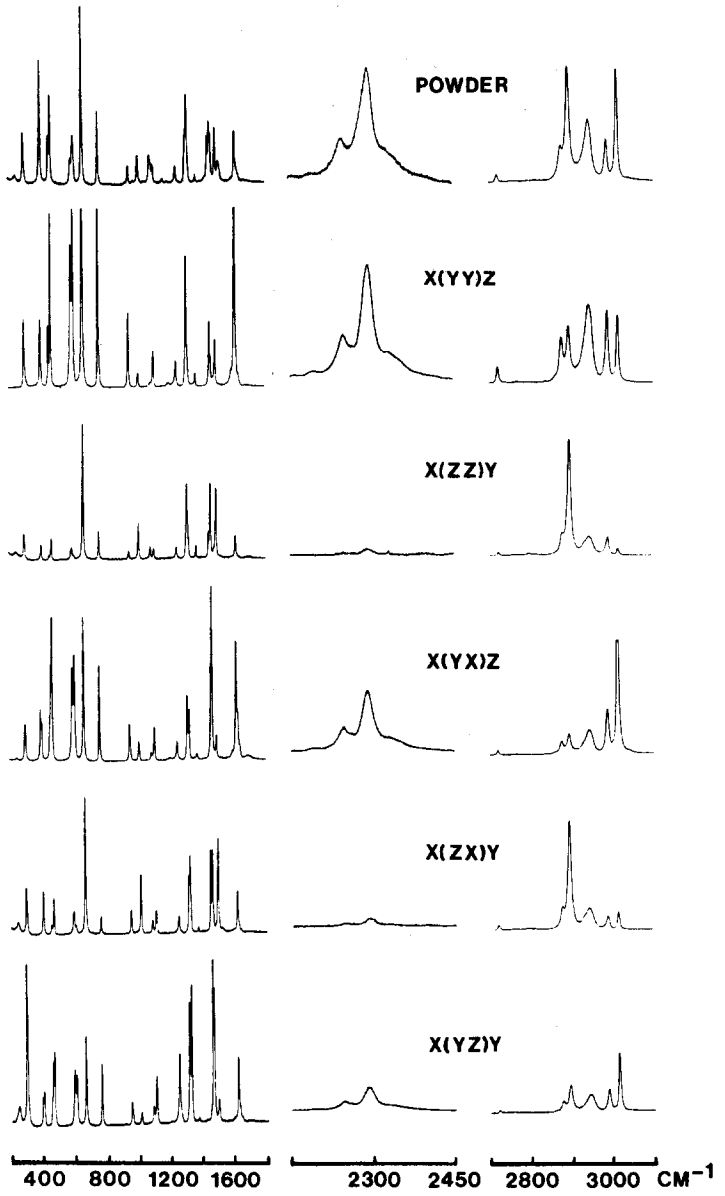

Fig. 4. Raman spectra of N-deuterated form II powder and single crystal.

lattice modes ($3A_g + 3B_g$) and 3 i.r.-active translatory lattice modes ($2A_u + 1B_u$). Where factor group splittings are observed, we have given the symmetry species for each component: bands of A_g symmetry appear in the xx, yy, zz, and xz spectra, whereas B_g bands appear in the xy and yz spectra; A_u bands are polarized parallel to y and B_u perpendicular. Though the ring atoms are very nearly co-planar [3–5], we have not tried to systematically classify the observed bands into in-plane and out-of-plane species because of the considerable inclination of the molecules to the x–y plane, which we estimate to be $\sim 20°$ in **I** and $\sim 25°$ in **II**. In the rest of this section, we will discuss our spectral assignments. After having established the assignments, we can then discuss in more detail in the following sections the spectral differences between the two forms. In general, the peptide group and ring modes were quite easily identified by comparison with cyclo(Gly-Gly) and by N-deuteration, and many of the side-chain modes were assigned by referring to analyses of L-alanine by other workers [13–15]. For reference, we note that the NH · · · OC dimensions in cyclo(Gly-Gly) are very close to those in **II** (Fig. 1): $R(\text{N} \cdots \text{O}) = 2.853$ Å, $\theta(\text{HNO}) = 7.5°$, $\theta(\text{CON}) = 121.8°$ [16].

Region above 2000 cm^{-1}. The NH stretch (str) and four CH str modes (per symmetry species) are found in this region. As in cyclo(Gly-Gly), the NH str band is relatively stronger in the i.r. than in the Raman, whereas the CH stretches are much more prominent in the Raman. These bands show distinct differences in **I** and **II**.

The NH str is easily assigned by N-deuteration. In **I**

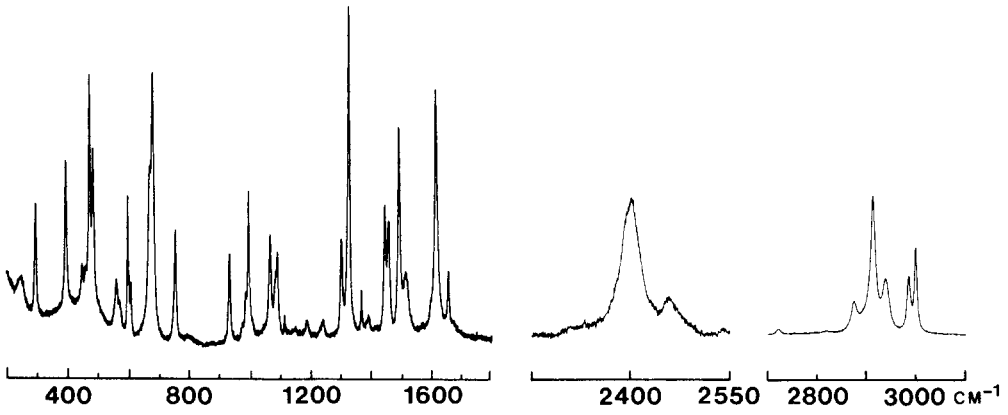

Fig. 5. Raman spectrum of N-deuterated form I powder.

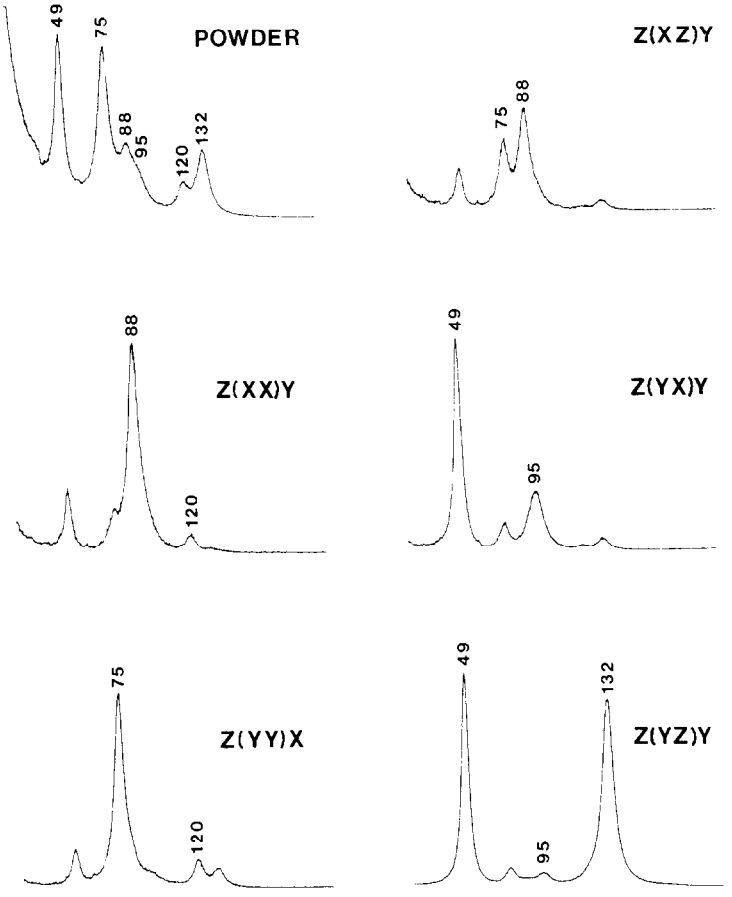

Fig. 6. Low frequency Raman spectra of form I powder and single crystal.

it forms a complex band with a main peak at 3247 cm^{-1} in the i.r. and 3239 cm^{-1} in the Raman. In its bandwidth and position, it is similar to the NH str band in α- and β-poly(L-alanine) [17]. A shoulder at 3258 cm^{-1} on the Raman peak becomes more distinct at liquid nitrogen temperature, and is fully resolved in the *xy* room temperature spectrum. Thus, whereas the main Raman peak is of A_g symmetry, the 3258 cm^{-1} band is B_g, giving a factor group splitting of 19 cm^{-1} if we consider only these two peaks. Both shift down at low temperature (LT), by 8 and 5 cm^{-1}, respectively; however, a weak A_g band at 3193 cm^{-1} shifts up on cooling, to 3197 cm^{-1}. The main i.r. peak also shifts down at LT by 11 cm^{-1} and sharpens appreciably,

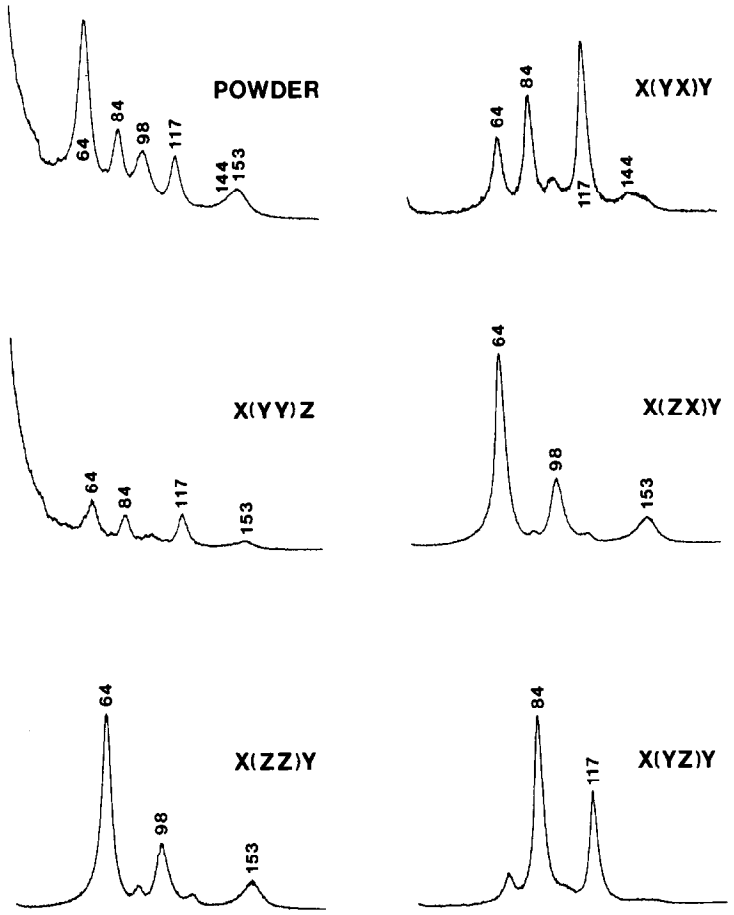

Fig. 7. Low frequency Raman spectra of form II powder and single crystal.

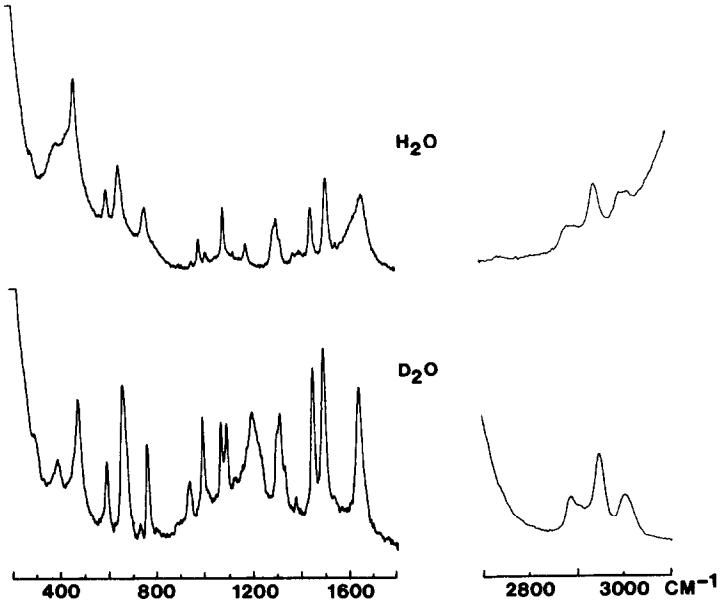

Fig. 8. Raman spectra of cyclo(D–Ala–L–Ala) in aqueous solution.

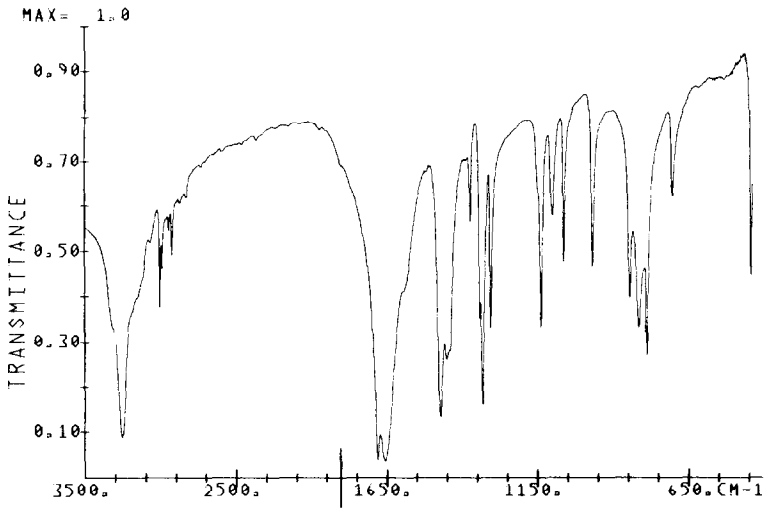

Fig. 9. I.r. spectrum of form I powder.

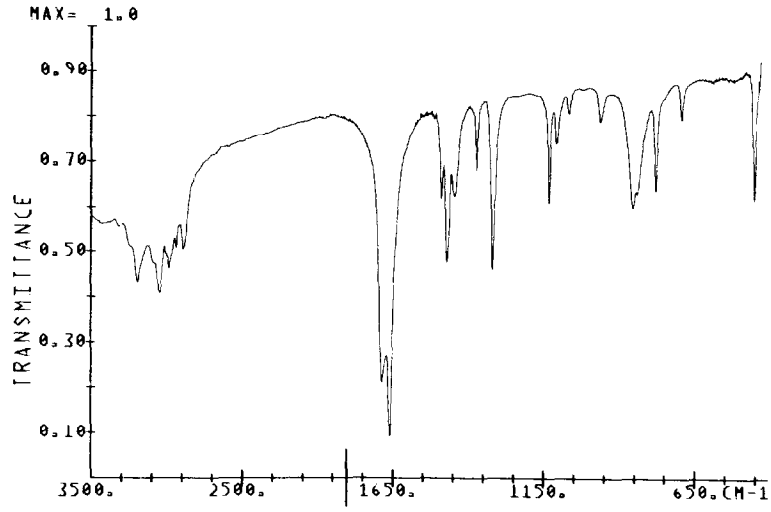

Fig. 10. I.r. spectrum of form II powder.

revealing a shoulder at 3222 cm^{-1}. Several other sub-bands are observed in both i.r. and Raman even at room temperature. In the i.r. these are at 3178, 3142, 3109, and 3058 cm^{-1}, suggesting a progression with a spacing of about 40 cm^{-1}.

The NH str band in **II** looks even more complex than in **I** and resembles closely that in cyclo(Gly-Gly). In the i.r., main sub-bands are found at 3192 and 3048 cm^{-1} (other sub-bands below 3000 cm^{-1} are weaker and difficult to distinguish from the CH stretches), and in the Raman broad, weak peaks are seen at 3164, 3107, and 3056 cm^{-1}. By comparison, in cyclo(Gly-Gly) we observed sub-bands at 3192, 3165, and 3046 cm^{-1} in the i.r. and at 3160, 3106, and 3035 cm^{-1} in the Raman. Also as in cyclo(Gly-Gly), at LT the i.r. bands sharpen appreciably, revealing more fine structure, and both the 3192 and 3048 cm^{-1} peaks shift down by 10 cm^{-1}. The Raman peaks are all strong in the *yy* spectrum; in addition, this spectrum shows a broad feature near 2914 cm^{-1}, among the CH str bands, that can be ascribed as part of the NH str complex in view of its similar polarization behavior and its absence in **II**–ND. Unlike in **I** and similar to cyclo(Gly-Gly), the B_g spectra show peaks in essentially the same positions as in the A_g spectra and with the same relative intensities. The strength of the NH str complex in the *xx* spectrum in **I** and in the *yy* spectrum in **II** is readily correlated with the direction of the NH bond in the two forms.

The ND str band is significantly narrower than the NH str, though again there is some fine structure. However, the difference in complexity between **I** and **II** is much less evident than for the NH str. In the i.r. in **I**,

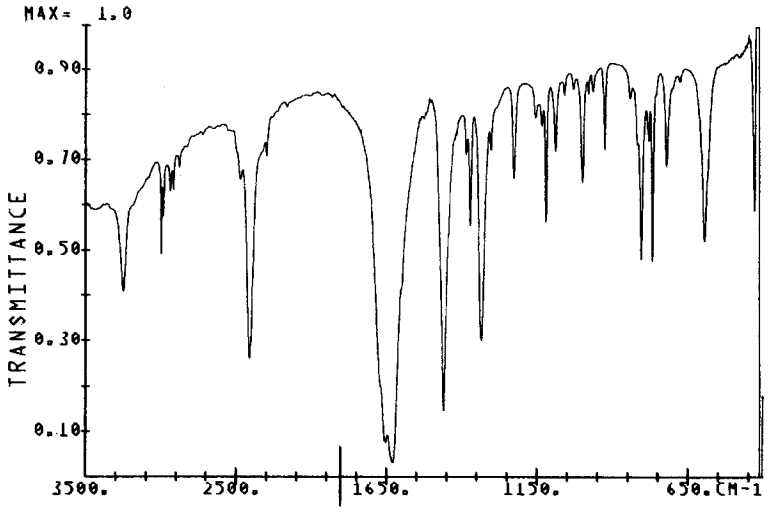

Fig. 11. I.r. spectrum of *N*-deuterated form I powder.

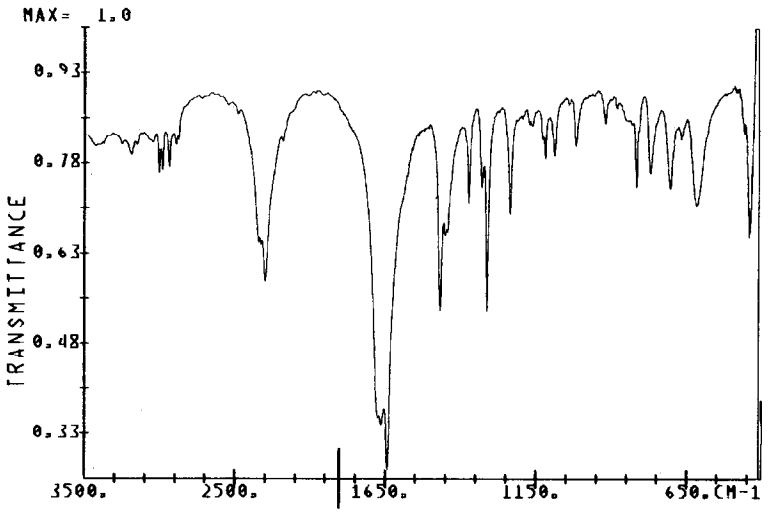

Fig. 12. I.r. spectrum of *N*-deuterated form II powder.

the main peak at 2411 cm^{-1} shifts to 2398 cm^{-1} at LT, while a shoulder at 2398 cm^{-1} becomes resolved at 2385 cm^{-1}. In **II** the main sub-band at 2298 cm^{-1} is resolved at LT into two peaks at 2287 and 2279 cm^{-1}, while the weaker sub-bands at 2344 and 2329 cm^{-1} move up to 2347 and 2331 cm^{-1}. Thus, we again see a tendency, on cooling, for the main peak to shift down by about 10 cm^{-1} and for additional sub-bands to become resolved. The main Raman sub-bands are at 2402 cm^{-1} (**I**) and 2294 cm^{-1} (**II**), similar to the i.r. The single-crystal spectra of **II**–ND show the same sub-bands in both A_g and B_g polarizations. The positions of the dominant sub-band imply a shift in the ND str frequency of about 100 cm^{-1} from **I** to **II**. A value for the shift of the NH str mode is obviously more difficult to arrive at in view of the complexity in **II**, but an estimate of $\sim \sqrt{2} \times 100 = 140\ cm^{-1}$ may be made, which would place the NH str frequency in **II** at about 3100 cm^{-1}.

To summarize, the NH str band is characterized by much fine structure. The band in **I**, which is similar to the NH str in poly(L-alanine) and other polypeptides, is much narrower than in **II**, where the band resembles that in cyclo(Gly-Gly) even in the sub-band positions. Going to low temperature causes marked sharpening and downward shifts of about 10 cm^{-1}, but some sub-bands shift up in frequency. An A_g–B_g splitting of about 19 cm^{-1} is seen in **I** but none is seen in **II**. There also seems to be no coincidence of the Raman and i.r. sub-band positions in either crystal form. From the narrower ND str bands, the frequency in **I** is found to be about 100 cm^{-1} higher than in **II**. These spectral

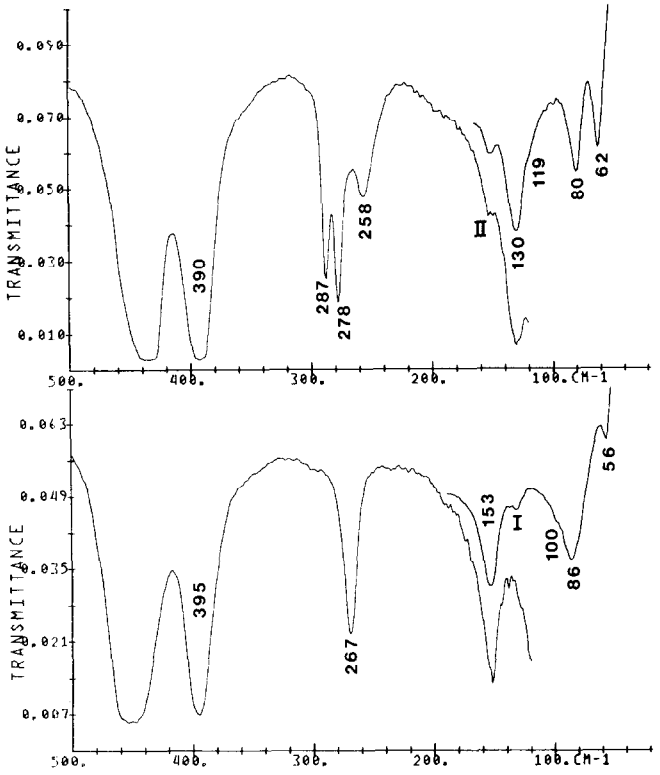

Fig. 13. Far-i.r. spectra of form I (top) and form II (bottom) powder.

differences are undoubtedly related to the different hydrogen bond patterns and strengths in the two forms.

In the CH str region five bands are found instead of the four expected. In I the Raman bands are at 2998, 2984, 2939, 2914, and 2877 cm^{-1}. The 2939 and 2877 cm^{-1} peaks have the same polarization behaviour and are evidently involved in a Fermi resonance. By comparison with the well-characterized CH str region of L-alanine [13–15], we therefore assign the 2998 and 2984 cm^{-1} peaks to the CH_3 antisymmetric stretches (as), the fundamental near 2939 cm^{-1} to CH_3 symmetric stretch (ss), and the 2914 cm^{-1} band to CH^{α} str. The corresponding frequencies in crystalline L-alanine are 3001, 2987, 2933, and 2968 cm^{-1}, respectively [13, 14]; the 2933 cm^{-1} peak is also part of a Fermi doublet, the other component being at 2877 cm^{-1}. The large difference in the CH^{α} str frequency in L-alanine and I may be somewhat less surprising when it is noted that in II its position is even lower, at 2893 cm^{-1}. Our assignment of this mode in cyclo(D-Ala-L-Ala) is supported by the single-crystal spectra: in I it is strong in *yy* polarization and weak in *xx*, whereas in II it is strong in *zz* and weak in *yy*, and furthermore the i.r. band in II has strong polarization along *z*; these observations are consistent with the direction of the CH^{α} bond in the two forms. Another prominent difference between I and II is that the CH_3 as at 2998 cm^{-1} in I moves up to 3011 cm^{-1} in II. There are also some intensity changes: in both Raman and i.r. the CH^{α} str is relatively stronger in I, and the two CH_3 as modes have more nearly equal Raman intensity in I but more nearly equal i.r. intensity in II (the i.r. CH stretches are best compared in the ND materials). In aqueous solution the CH^{α} str and higher frequency CH_3 as Raman bands become diffuse, with frequencies closer to those of form II. Because the other bands are also shifted, we cannot conclude from the CH str region that the form II conformation predominates in solution. As we will see, however, the H^{α} bend modes do allow such a determination.

1700–1200 cm^{-1} *region.* Eight modes are found in this region: three peptide group vibrations (CO str, CN str, and NH in-plane bend), three CH_3 bends, and the two orthogonal H^{α} bend modes.

The CO str, observed in the 1600 cm^{-1} region, shows an *A–B* splitting in all spectra of the crystalline samples; in solution a singlet is seen. (An additional weak peak is seen near 1580 cm^{-1} in the Raman and i.r. spectra of I–NH. The Raman single-crystal spectra show this band to be in Fermi resonance with the A_g CO str. Because of its weakness, we will neglect its effect.) The splittings (*A–B* and *g–u*), positions, and relative intensities are distinctly different in the various spectra. For instance, looking at the Raman spectra, we see in I a larger A_g–B_g splitting (48 cm^{-1} versus 20 cm^{-1}) and a higher relative intensity than in II, where the band is similar to that in cyclo(Gly-Gly).

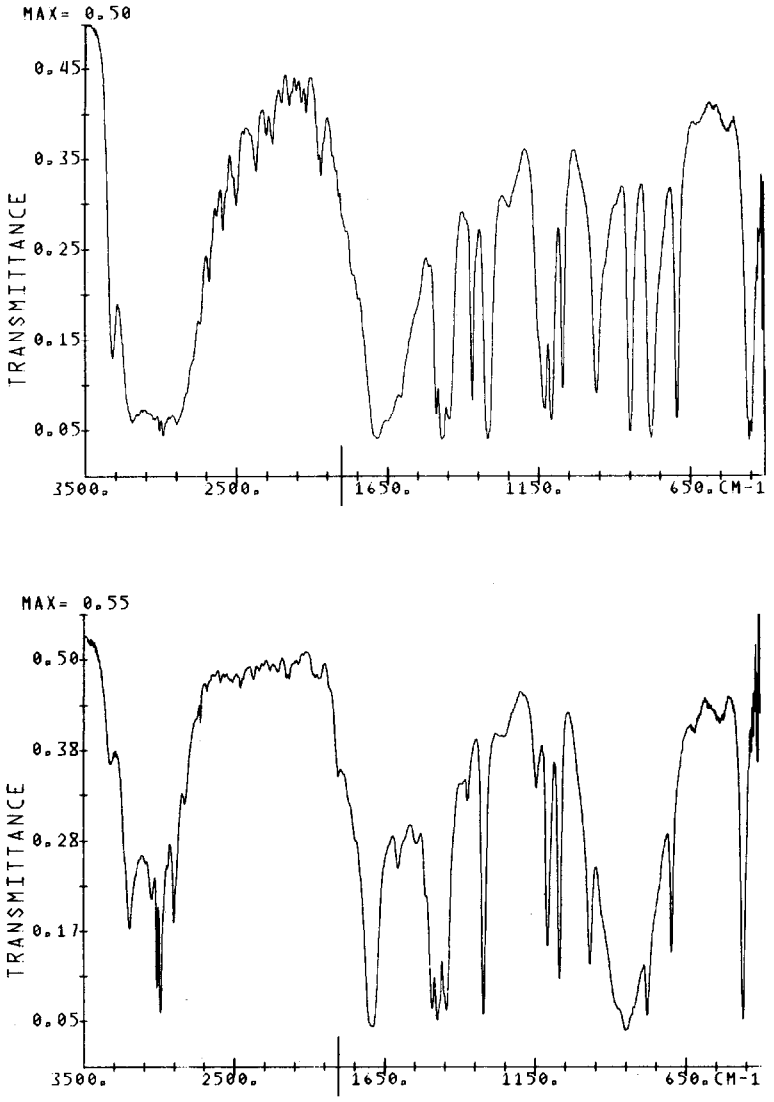

Fig. 14. I.r. spectra of form II single crystal, (100) section. Top: Electric vector parallel to *b*. Bottom: Electric vector parallel to *c*.

The single-crystal spectra show the B (B_g or B_u) component to be higher in frequency than the A (A_g or A_u). This result is conclusive for the Raman components and for the i.r. components of **II**, but is less so for the i.r. doublet of **I** because of strong absorption. The large (factor of about 9) difference in integrated intensity of the i.r. components in **I** suggests that an *ab initio* calculation of the transition moment direction would be useful. A calculation with the STO-3G basis of the dipole moment derivative for the CO str mode in cyclo(Gly-Gly) gives a transition moment oriented at about 16° from the CO bond towards the N → C direction. This orientation would yield a ratio of the A_u to B_u intensities in **I** of about 4, which would confirm our assignment.

The CN str mode is readily assigned to strong bands near 1520 cm^{-1} (Raman) and near 1470 cm^{-1} (i.r.) in view of its nearly identical positions in cyclo(Gly-Gly). As we have noted [1], this mode can be described as mainly an out-of-phase $C^{\alpha}CN$ str (Fig. 15), with much less NH in-plane bend contribution than in the *trans* amide II mode; hence its relatively higher Raman intensity and smaller shift on N-deuteration compared to the amide II. The band positions in **I** and **II** are nearly the same, indicating little sensitivity to the hydrogen bond structure, and the persistence of the large g–u splitting in solution suggests an intramolecular rather than intermolecular origin.

N-deuteration allows location of the NH in-plane bend (ib) at 1395 cm^{-1} (**I**) and 1428 cm^{-1} (**II**) in the Raman and at 1435 cm^{-1} (**I**) and 1488 cm^{-1} (**II**) in the i.r. The large shifts between **I** and **II** show a strong

sensitivity to the hydrogen bond. The positions in **II** are close to those in cyclo(Gly-Gly), particularly in the C-deuterated derivative of the latter, where the absence of coupling with CH_2 bend in the Raman leaves the NH ib at 1437 cm^{-1}. We note that the i.r. band in **II** is resolved from the CN str even at room temperature, unlike in cyclo(Gly-Gly), where its overlap with CN str hindered definitive assignment of the NH ib mode until our work [1]. Despite being near to the CH_3 bend modes, there does not seem to be significant coupling: the Raman CH_3 bends hardly shift on N-deuteration. The ND ib does interact strongly with NC^{α} str and H^{α} bend, according to our calculations.

The two CH_3 antisymmetric bends (ab), at around 1450 cm^{-1}, are more clearly seen in the Raman spectra; the i.r. bands are not resolved from each other except in **II**-ND. In the Raman the higher frequency CH_3 ab in **II** is stronger than the lower frequency CH_3 ab but is nearly equally intense in **I**, a trend that is also shown by the two CH_3 as Raman modes.

Like the CH_3 ab's, the CH_3 symmetric bend (sb) has essentially the same frequency in **I** as in **II**, at about 1370 cm^{-1}. It is weak and sharp in all spectra. The calculations show all three CH_3 bend modes to be highly localized.

The assignment of the bands in the 1300–1340 cm^{-1} region to the two H^{α} bend (b) modes is based on the normal mode calculations and on comparison with L-alanine [13–15]. Figure 15 shows these modes to be relatively localized, with the higher frequency mode involving motion of the H^{α} atom mainly in the $H^{\alpha}C^{\alpha}C^{\beta}$ plane. The H^{α} b modes show marked differences between **I** and **II**. Looking first at the Raman data, we see in **I** a very strong 1326 cm^{-1} band and a much weaker 1304 cm^{-1} peak, whereas in **II** the intensities are nearly equal and the separation of the two bands, at 1313 and 1300 cm^{-1}, has decreased considerably. In the i.r. spectra a similar decrease of the separation, from 33 cm^{-1} to 9 cm^{-1}, occurs but the higher frequency band remains much more intense than the other. On N-deuteration, coupling of the i.r. H^{α} b vibrations with ND ib near 1230 cm^{-1} is indicated by the upward shifts in the H^{α} b bands, which reduces the H^{α} b separation in **I**–ND to the point of overlap and increases it in **II**–ND. This interaction with ND ib is qualitatively reflected by the calculations; note, however, that no significant coupling with NH ib is indicated, in distinction to the *trans* amide, where such coupling is widespread. The Raman spectrum in H_2O solution shows three peaks in the H^{α} b region. These can be explained by the presence of both form **I**- and **II**-type molecules: the 1325 cm^{-1} peak is due to **I**, the 1311 cm^{-1} peak to **II**, and the 1300 cm^{-1} peak to both **I** and **II**. Molecules with form **II** conformation predominate, as shown by the relative intensities of the 1311 and 1325 cm^{-1} peaks. The i.r. solution spectrum may be similarly interpreted: the 1324, 1312, and 1294 cm^{-1} bands are attributed to **I** + **II**, **II**, and **I**, respectively. Similar statements may be made about the D_2O solution spectra. Thus, the differences in the H^{α} b frequencies in **I** and **II** occur in solution also and are therefore of intramolecular origin. In particular, they are not due to coupling with an NH ib vibration that occurs at different frequencies in **I** and **II**. Further indication of a structural dependence of the H^{α} b

II-ND. In the Raman the higher frequency CH_3 ab in **II** is stronger than the lower frequency CH_3 ab but is

1200–900 cm^{-1} *region.* Four modes occur in this region: NC^{α} str, $C^{\alpha}C^{\beta}$ str, and two CH_3 rock vibrations. Since four well-separated bands are observed, the assignment is straightforward, especially because the calculated frequencies agree well with those observed. The NC^{α} str is seen from the calculations to be strongly mixed with H^{α} b. N-deuteration shifts all four modes to lower frequencies, the magnitudes being smallest for the $C^{\alpha}C^{\beta}$ str ($\sim$ 20 cm^{-1}) and largest for the Raman NC^{α} str ($\sim$ 100 cm^{-1}); the CH_3 rock shifts range up to 60 cm^{-1}. These shifts, which are quite well reproduced by the calculations, arise from new mixings involving ND ib. The main structure-sensitive feature in this region is the change in the Raman and i.r. intensities of the CH_3 rock bands when the higher frequency mode moves up by about 10 cm^{-1} from **I** to **II**. The largest difference in frequency between **I** and **II** in this region is the 20 cm^{-1} upward shift of the i.r. CH_3 rock at 998 cm^{-1} in **I**–ND; as a result the two i.r. peaks at 1017 and 994 cm^{-1} in D_2O solution can be attributed to types **II** and **I** molecules, respectively, further evidence that the molecules exist in solution in two discrete conformations.

900–500 cm^{-1} *region.* From our cyclo(Gly-Gly) results, we expect in this region three peptide group vibrations—NH out-of-plane bend, CO out-of-plane bend, and the Raman-active CO in-plane bend—and a ring stretch mode and an i.r.-active ring deformation (def) mode, making a total of four bands in each spectrum. The observed bands are sufficiently similar to those in cyclo(Gly-Gly) to be readily assigned, except for the CO out-of-plane bend (ob).

In cyclo(Gly-Gly) the CO ob is a weak band around 560 cm^{-1} in both i.r. and Raman spectra. We assign this mode in **I** and **II** to bands near 690 cm^{-1} (i.r.) and 670 cm^{-1} (Raman), the much higher frequencies and intensities being due to coupling with ring and side-chain deformations. These couplings, which are negligible in the more nearly planar cyclo(Gly-Gly) structure, are confirmed by the calculations. (The poor frequency agreement, with the Raman CO ob lower than CO ib, contrary to our assignment, is no doubt due to the absence of force constants for these interactions.) Furthermore, on N-deuteration the CO ob bands shift up whereas the other bands in this region decrease in frequency, and the i.r. band in **II**–ND becomes more intense and shows stronger z polarization. Similar changes were noted for cyclo(Gly-Gly) and are due to interaction of CO ob with ND ob. The small difference in frequency between **I** and **II** shows this mode to be not especially sensitive

Table 1. Observed Raman and i.r. frequencies (in cm^{-1}) of cyclo(D-Ala-L-Ala) in forms I and II and in aqueous solution

Assignment	I		II		I–ND		II–ND		H_2O		D_2O	
	Raman	i.r.	Raman	i.r.	Raman	i.r.	Raman	i.r.	Raman	i.r.	Raman	i.r.
NH(ND) str	3258sh†	3312sh	3164w*	3192s	2456w	2470w	2331sh	2344w				
	3239m*	3247vs	3107w*	3048s	2402m	2411s	2294m	2329w				
	3193vw*		3056w*		2395sh	2398sh	2248w	2298s				
CH_3 asym str	2998m	2997m	3011s	3010w	2998m	2997m	3010s	3007w	3015w		3012sh	
CH_3 asym str	2984m	2981w	2985m	2985w	2984m	2982w	2985m	2985w	2999m		2999m	
CH_3 sym str	2939m	2938vw	2941s	2938w	2938m	2937w	2941s	2939w	2945m		2946m	
CH^{α} str	2914s	2916w	2893s	2896w	2914s	2915w	2893s	2894vw	2903w		2905w	
overtone	2877m	2868vw	2872sh	2878sh	2875m	2876vw	2875m	2876vw	2887m		2886m	
CO str	1678w†	1676s†	1668vw†	1687vs†	1658w	1655s	1624sh†	1664vs†	1664m		1645m	1643s
	1630m*	1651vs*	1648w*	1660vs*	1616m	1630vs	1611m*	1643vs*				
Ring str	1523s	1468s	1516s	1470s	1495m	1459s	1490m	1467s	1517m	1475s	1500m	1466s
NH(ND) ipb	1395m	1435m	1428m	1488m	1245w	1225m	1244m	1234m	1404vw		1228sh	
CH_3 asym bend	1463m†		1463m†		1460m		1462m†					
	1460sh*	1447m	1455m*	1443m		1451sh	1454m*	1451m	1455m		1455m	1449sh
	1448m		1446m		1448m	1442sh	1443m	1442m			1449sh	
CH_3 sym bend	1370w	1368m	1366w	1372m†	1370w	1370m	1366w	1372m	1379vw	1380w	1381vw	1381w
				1367sh*								
H^{α} bend	1326*	1336w			1330vs		1322sh†	1329m	1325vw	1324s	1336w	1334w
	1320sh†	1327s	1313s	1318s		1333s	1314s*	1311s	1311m	1312sh	1317m	1313w
	1304m	1299m	1300s	1309sh	1304m		1304sh		1300sh	1294sh	1304sh	
NC^{α} str	1195m†											
	1191m*	1132s	1190m	1130s	1094m	1119m	1102m	1119m	1186w	1132w	1096m	1098vw

$C^{\alpha}C^{\beta}$ str	1088m	1095m	1093m	1106m* 1104m†	1070m	1087m	1081m	1088m	1093m	1093vw	1073m	1087vw
CH_3 rock	1013w	1057m	1023m	1068w* 1065m†	999m	998m	1009m	1018m	1020w	1060vw	996m	1017vw 994vw
CH_3 rock	989m	962m	990w	964w† 958m*	935m	924m	949m	920m	991w		940w	923vw
NH(ND) opb	814vw† 793w*	808s	826vw	853s	574w 561m	593s	591w	616s				
Ring str	752m	839m	762m	839m	757m	804m	760m	817m	767m		767m	808vw
CO opb	672vs	698m	661vs	692m	683vs	719m	663vs	704m	662m		668m	
CO ipb	612m	437s† 428w*	616s	455w† 451s*	599m	427s 415w	606m	449w† 441s*	610m		597m	
Ring def	489m† 474m*	782m	468s	778s* 775w†	485m 473s	766m	466m* 461sh†	770m	481m		481m	770vw
Ring def	460m		464s		449w		454m		448sh		459sh	
C^{β} bend	398m	390m	404s* 397w†	395m	395m	379w	402m	384m	404m		393w	
C^{β} bend	298m	287w* 278w†	300m	268w* 265w†	296m	286w	298m	269w* 265w†	300vw		299vw	
Ring tor	252w	258w	247w		249w		247w					
$C^{\alpha}C^{\beta}$ tor		~226		~226								
Ring tor		130w		153w				152w				
Lattice	132s† 120m* 95w† 88m* 75vs* 49vs†	119sh* 80w† 62w*	153m* 144w† 117m† 98m* 84m† 64vs*	~100sh* 86w† 56w*	128s 117m 94w 85m 73vs 48vs		150m* 140w† 115m† 96m* 82m† 63vs*					

* A_g or A_u species.
† B_g or B_u species.

Table 2. Calculated intramolecular modes of II and II–ND, without intermolecular force constants

Obs.* (cm^{-1})	Calc. (cm^{-1})	Potential energy distribution (> 10%)†
		II (A_g)
~3100	3074	NH str(99)
3011	2994	CH_3 as2(98)
2985	2989	CH_3 as1(98)
2941	2916	CH_3 ss(99)
2893	2903	CH^{α} str(98)
1658	1611	CO str(29), NH ib(26), CN str(22), NC^{α} str(15)
1516	1531	$C^{\alpha}C$ str(48), CO ib(18), CN str(16)
1459	1471	CH_3 ab1(46), CH_3 ab2(42)
1446	1461	CH_3 ab1(44), CH_3 ab2(43)
1428	1435	NH ib(64), CO str(16)
1366	1369	CH_3 sb(96)
1313	1315	H^{α} b1(42), H^{α} b2(15), NC^{α} str(13)
1300	1275	H^{α} b2(40), H^{α} b1(23), CO str(14)
1190	1173	H^{α} b2(38), NC^{α} str(19), CO str(13)
1093	1071	$C^{\alpha}C^{\beta}$ str(57), CH_3 r1(28)
1023	1016	CH_3 r2(31), CH_3 r1(21), H^{α} b1(14)
990	983	CH_3 r2(31), $C^{\alpha}C^{\beta}$ str(13), CH_3 r1(13)
826	825	NH ob(54)
762	741	$NC^{\alpha}C$def(17), CH_3 r1(16), $C^{\alpha}C$ str(14), CO ob(14)
616	639	CO ib(48), C^{β}b2(20), CN str(16)
661	612	CO ob(32), $C^{\alpha}C$ str(18)
471	479	CNC^{α} def(25), C^{β} b1(18)
464	424	$C^{\alpha}CN$ def(27), NC^{α} str(21), C^{β} b1(19), $NC^{\alpha}C$ def(11)
401	362	C^{β} b2(35), $NC^{\alpha}C$ def(15)
300	297	C^{β} b2(34), $NC^{\alpha}C$ def(18), CO ob(14), C^{β} bl(13)
—	242	$C^{\alpha}C^{\beta}$ tor(96)
247	149	$C^{\alpha}C$ tor(53), NC^{α} tor(37), CN tor(32)
		II (A_u)
~3100	3078	NH str(99)
3010	2994	CH_3 as2(98)
2985	2989	CH_3 as1(98)
2938	2916	CH_3 ss(99)
2896	2903	CH^{α} str(98)
1674	1671	CO str(57), NH ib(21), $C^{\alpha}CN$ def(14)
1488	1514	NH ib(56), CO str(16)
1443	1470	CH_3 ab2(63), CH_3 ab1(25)
1443	1468	CH_3 ab1(57), CH_3 ab2(23)
1470	1428	$C^{\alpha}C$ str(21), CN str(18), CO ib(17)
1370	1369	CH_3 sb(98)
1318	1311	H^{α} b1(52)
1309	1300	H^{α} b2(59)
1130	1155	H^{α} b2(33), CH_3 r2(19), NC^{α} str(11)
1106	1111	$C^{\alpha}C^{\beta}$ str(52)
1066	1047	CH_3 r1(45), H^{α} b1(23), $NC^{\alpha}C$ def(11)
951	962	CH_3 r2(41), NC^{α} str(16), CNC^{α} def(12)
839	854	CH_3 r1(21), $C^{\alpha}C^{\beta}$ str(19)
853	829	NH ob(44), CH_3 r2(11)
778	775	NH ob(31), $C^{\alpha}C^{\beta}$ str(16), $C^{\alpha}CN$ def(14)
692	626	CO ob(63), $NC^{\alpha}C$ def(12)
453	433	$NC^{\alpha}C$ def(35), CO ib(19), CO ob(12)
395	358	CO ib(47)
267	272	C^{β} b2(62), CO ob(17)
~226	239	$C^{\alpha}C^{\beta}$ tor(96)
~260	149	CN tor(39), NH ob(15)
153	82	$C^{\alpha}C$ tor(48), NC^{α} tor(34)
		II–ND (A_g)
3010	2994	CH_3 as2(98)
2985	2989	CH_3 as1(98)
2941	2916	CH_3 ss(99)
2893	2903	CH^{α} str(98)
~2300	2262	ND str(97)
1618	1590	CO str(37), CN str(24), NC^{α} str(16)
1490	1525	$C^{\alpha}C$ str(47), CO ib(18), CN str(16)
1458	1470	CH_3 ab1(51), CH_3 ab2(38)
1443	1460	CH_3 ab2(51), CH_3 ab1(38)

Table 2 (*Contd.*)

1366	1369	CH_3 sb(96)
1318	1313	H^{α} b1(42), H^{α} b2(14), NC^{α} str(13)
1304	1276	H^{α} b2(49), H^{α} b1(20)
1244	1224	CO str(24), ND ib(22), H^{α} b2(20), NC^{α} str(18)
1102	1094	ND ib(34), CH_3 r2(32), H^{α} b2(15)
1081	1070	$C^{\alpha}C^{\beta}$ str(57), CH_3 r1(30)
1009	1002	CH_3 r1(33), H^{α} b1(22), $C^{\alpha}C^{\beta}$ str(19)
949	939	CH_3 r2(38), ND ib(28), NC^{α} str(12)
760	745	$NC^{\alpha}C$ def(21), CH_3 r1(18), CO ob(14), ND ob(12), $C^{\alpha}C$ str(11)
591	651	ND ob(35), C^{β} b2(11)
663	612	CO ob(19), CN str(16), CO ib(12), ND ob(12)
606	599	CO ib(33), CO ob(16), $C^{\alpha}C$ str(14)
464	472	CNC^{α} def(26), C^{β} b1(18)
454	424	$C^{\alpha}CN$ def(27), NC^{α} str(21), C^{β} b1(20), $NC^{\alpha}C$ def(11)
402	349	C^{β} b2(34), $NC^{\alpha}C$ def(17)
298	297	C^{β} b2(35), $NC^{\alpha}C$ def(17), CO ob(14), C^{β} b1(13)
—	242	$C^{\alpha}C^{\beta}$ tor (96)
247	143	$C^{\alpha}C$ tor(53), NC^{α} tor(39), CN tor(35).
		II–ND (A_u)
3007	2994	CH_3 as2(98)
2985	2989	CH_3 as1(98)
2939	2916	CH_3 ss(99)
2894	2903	CH^{α} str(98)
~2300	2272	ND str(96)
1654	1647	CO str(72), $C^{\alpha}CN$ def(17)
1451	1472	CH_3 ab1(76)
1442	1469	CH_3 ab2(76)
1467	1424	$C^{\alpha}C$ str(23), CO ib(16), CN str(15)
1329	1370	CH_3 sb(37), H^{α} b1(23), $C^{\alpha}C^{\beta}$ str(12)
1372	1367	CH_3 sb(63)
1311	1301	H^{α} b2(64)
1234	1231	H^{α} b1(35), ND ib(26)
1119	1146	H^{α} b2(32), CH_3 r2(22)
1088	1079	$C^{\alpha}C^{\beta}$ str(48), CH_3 r1(26)
1018	1009	CH_3 r1(34), H^{α} b1(22), ND ib(14)
920	932	CH_3 r2(47), NC^{α} str(15)
817	808	$C^{\alpha}C^{\beta}$ str(23), CH_3 r1(16), $NC^{\alpha}C$ def(13)
770	777	ND ib(21), $C^{\alpha}CN$ def(14)
616	669	ND ob(76), CO ob(24)
704	618	CO ob(44), $NC^{\alpha}C$ def(16)
445	399	CO ib(37), $NC^{\alpha}C$ def(20)
384	347	CO ib(29), $NC^{\alpha}C$ def(14), C^{β} b2(12)
267	271	C^{β} b2(60), CO ob(18)
—	239	$C^{\alpha}C^{\beta}$ tor(96)
—	145	CN tor(41), ND ob(13)
—	82	$C^{\alpha}C$ tor(48), NC^{α} tor(35)

*From crystalline samples. Where A–B splittings are observed, average frequency is listed.

†Abbreviations: str = stretch, as = antisymmetric str, ss = symmetric str, b = bend, ab = antisymmetric b, sb = symmetric b, def = deformation, ib = in-plane b, ob = out-of-plane b, r = rock, tor = torsion.

to the hydrogen bond structure, perhaps because of its highly mixed character.

The NH ob mode, easily identified by N-deuteration, appears in **II** at nearly the same positions as in cyclo(Gly-Gly), 853 cm^{-1} (i.r.) and 826 cm^{-1} (Raman). In **I** this mode is at 808 cm^{-1} (i.r.) and 804 cm^{-1} (Raman); thus, the fractional shift of this mode from **I** to **II** is comparable to that of the NH str. The Raman ND ob mode is much more intense than the NH ob because of coupling with CO ob, as we saw also in cyclo(Gly-Gly).

The remaining two i.r. bands in this region, near 839 and 780 cm^{-1}, are easily assigned to the ring str and def vibrations. The calculations show these modes to be highly mixed. The $C^{\alpha}C$ (or ring) str mode in the Raman is near 760 cm^{-1}, its much weaker intensity compared to that in cyclo(Gly-Gly) being due to coupling with CO ob and other coordinates. Finally, the Raman CO ib is placed at 612 cm^{-1} in **I** and at 616 cm^{-1} in **II**, essentially the same position as in cyclo(Gly-Gly).

Intramolecular modes below 500 cm^{-1}. Six internal modes are expected in each spectrum below 500 cm^{-1}:

Table 3. Calculated lattice modes of I and II, in cm^{-1}

Symmetry	I Calc.	I Obs.	II Calc.	II Obs.
A_g	136	120	147	153
	95	88	114	98
	73	75	75	64
B_g	132	132	146	144
	111	95	114	117
	52	49	85	84
A_u	142	119	123	100
	77	62	72	56
B_u	80	80	80	86

two C^β bends and $C^\alpha C^\beta$ torsion; in addition, two ring deformations and one ring torsion in the Raman, and CO in-plane bend and two ring torsions in the i.r. The Raman modes are well separated from the lattice modes and are easily assigned, except for the $C^\alpha C^\beta$ torsion (tor) which is not observed. In the i.r. the location of one of the ring tor modes among the lattice modes makes our assignment of this ring tor vibration as well as of the translatory lattice modes tentative at present.

The Raman-active ring def modes are seen at nearly the same frequencies as in cyclo(Gly-Gly), around 470 cm^{-1}, and also with an observable splitting of the higher frequency mode.

The i.r. band in the 400 cm^{-1} region is clearly the CO ib mode in view of its similar position in cyclo(Gly-Gly). Its frequency in II is 20 cm^{-1} higher than in I, a fractional shift of 4.6%. Thus, the i.r.-active CO ib seems much more sensitive to the hydrogen bond structure than does its Raman counterpart.

The two measured C^β b frequencies near 400 and 300 cm^{-1} agree well with the calculated values. The lower frequency C^β b shows an i.r. splitting that is clearly seen in the powder spectrum of I, but which in II requires polarized spectra to be resolved. The C^β b modes are distinguished from the other low frequency i.r. and Raman bands by their insensitivity to cooling.

The remaining internal modes in this region are the torsions. The weak, broad Raman band near 250 cm^{-1} corresponds to the ring tor in cyclo(Gly-Gly). The $C^\alpha C^\beta$ tor is also expected in the 200 cm^{-1} region, but no other peak is observed. The data on L-alanine are not a useful guide here because of disagreements in the assignments [14, 15]. In the i.r. this mode is expected to be very weak, and we tentatively assign it to a weak band at 226 cm^{-1} that is seen only in the low-temperature spectra of I and II. The Raman mode may very likely be overlapped with the ring tor at 250 cm^{-1}. Thus, except for the $C^\alpha C^\beta$ tor, all Raman-active internal modes are satisfactorily assigned.

One of the i.r. ring tor modes is also expected in the 200–300 cm^{-1} range and is assigned to the broad 258 cm^{-1} band in I, which sharpens considerably and shifts up by 5 cm^{-1} on cooling. In II no corresponding peak is apparent. It is possible that the 10 cm^{-1} downward shift of the C^β b mode in II has resulted in an overlap with the ring tor. The reason for the appreciable i.r. intensity of the ring tor mode, at least in I, compared to that in cyclo(Gly-Gly) is not obvious and may be checked by an *ab initio* calculation; we recall that in the latter compound we placed this mode at 285 cm^{-1} on the basis of neutron scattering data [18] because no i.r. peak was seen. The lower frequency i.r. ring tor may be mixed with the lattice vibrations. We will therefore merely mention that we assign it to bands at 130 cm^{-1} (I) and 153 cm^{-1} (II), and defer further discussion until we consider the translatory lattice modes.

Lattice modes. The six rotatory lattice vibrations are readily classified into A_g or B_g species using the single-crystal spectra. They are very different in frequency and relative intensity in I and II, and also in cyclo(Gly-Gly), as would be expected. They all sharpen at low temperature and shift by up to 3 cm^{-1} in I and up to 7 cm^{-1} in II.

The i.r. translatory lattice modes are not as conclusively assigned. Because one of the ring tor modes falls in the same region, we expect to find four bands. The 130 cm^{-1} band in I shows significant intensity in the single-crystal spectra both parallel and perpendicular to y and is therefore most likely an internal mode. The 153 cm^{-1} peak in II is then assigned as the corresponding ring tor in the other crystal form; the large shift may be caused by coupling with lattice vibrations, an interaction that is indicated by our calculations. Of the remaining bands, the 80 cm^{-1} (I) and 86 cm^{-1} (II) peaks show clear perpendicular dichroism and can be assigned to the B_u lattice mode. The 62 cm^{-1} (I) and 56 cm^{-1} (II) peaks are apparently polarized parallel to y and are accordingly one of the A_u lattice vibrations. Weak bands seen near 119 cm^{-1} in I and 100 cm^{-1} in II are then the other A_u lattice mode. What makes our assignment of the A_u modes quite tentative at present is that the polarizations of the 119, 100 and 56 cm^{-1} peaks are not definitive because of their weakness. Also, at low temperature the 62 cm^{-1} peak in the powder spectrum of I is a doublet; whether the other band is due to a form II impurity is not yet certain.

Our calculated lattice-mode frequencies (Table 3) using MOMANY *et al.*'s [12] atom–atom potential agree well with the A_g and B_g observed values, as was found also for cyclo(Gly-Gly). The relatively well-assigned B_u lattice mode is also well reproduced, and the poorer agreement of the higher frequency A_u mode may be because of coupling with the ring torsions. The good performance of this potential further supports our conclusion [2] that this set of parameters is very satisfactory for peptide crystals. We also note that, using the crystal-packing program MCA [19], we have minimized the energy of forms I and II using these potential parameters by allowing rigid body rotations and translations. We find that form I is slightly more stable than II, with crystal energy of −9.924 kcal/mole versus −9.452 kcal/mole.

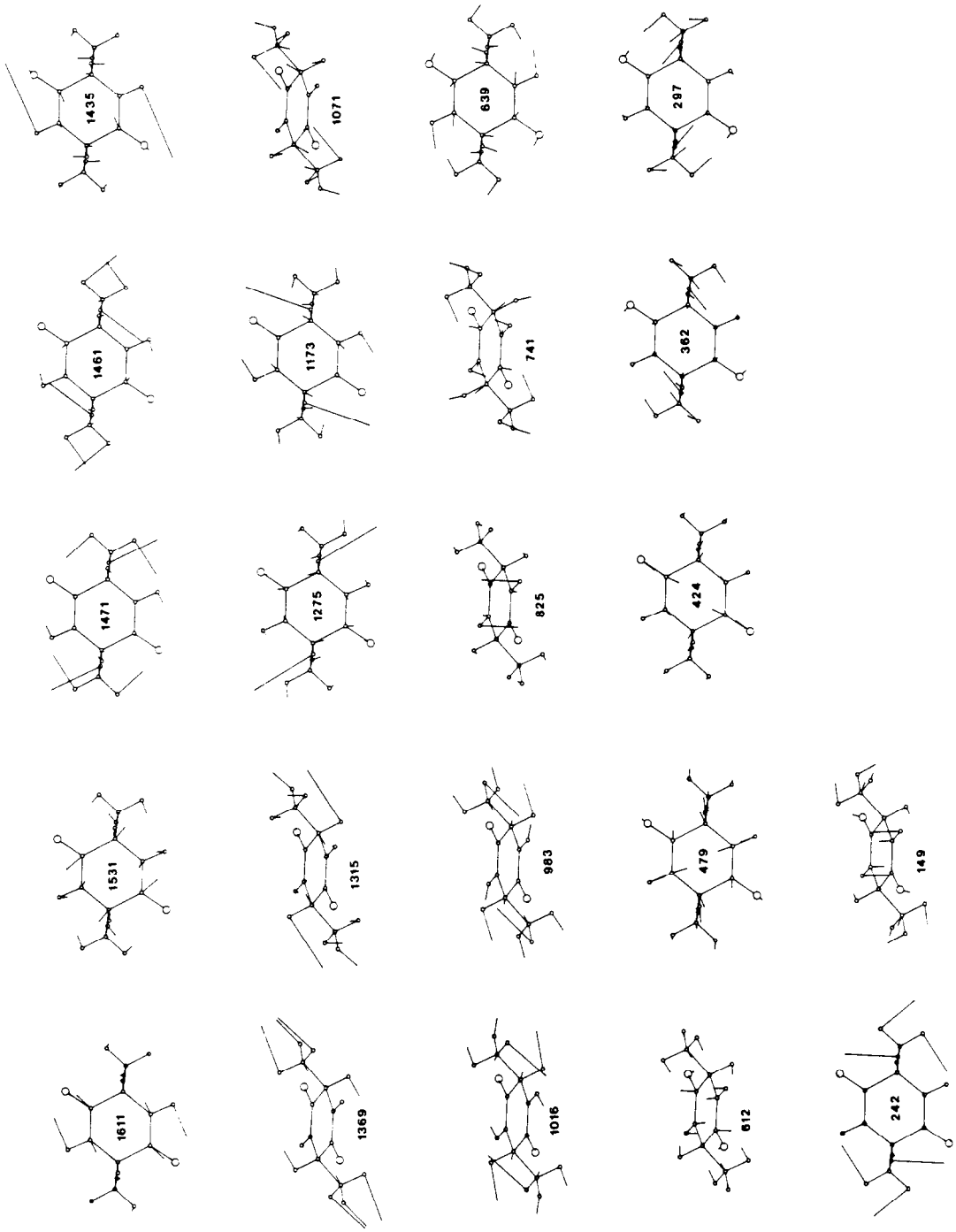

Fig. 15. Raman-active intramolecular modes of form **II**. Oxygen atoms drawn extra large. Calculated frequencies in cm^{-1} shown.

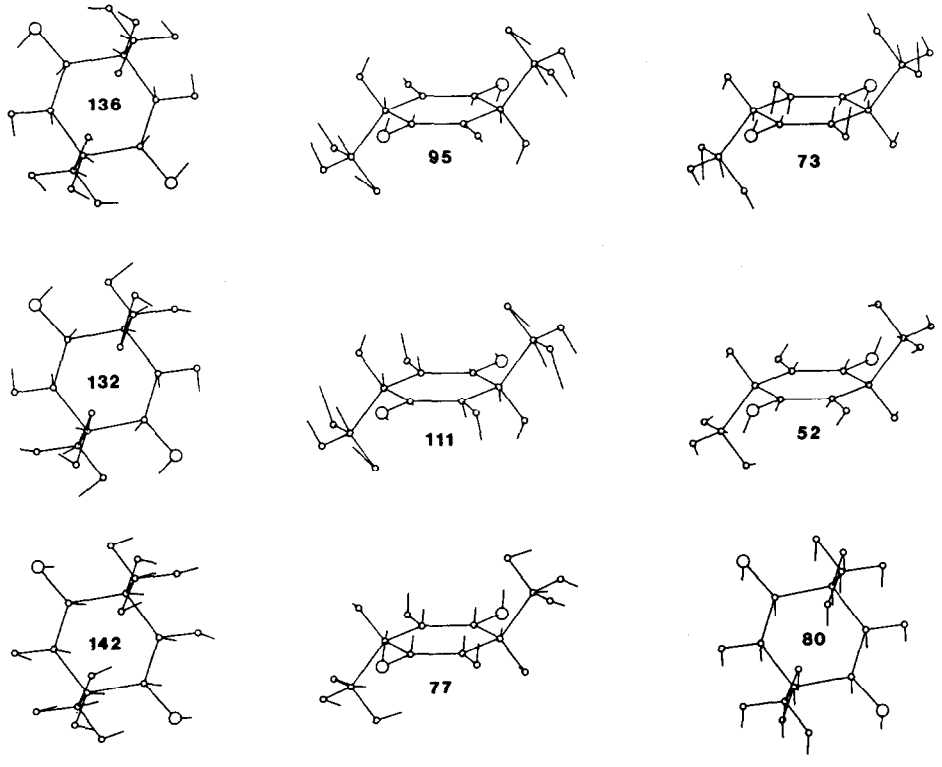

Fig. 16. Lattice modes of form I. Oxygen atoms drawn extra large. Top row: A_g. Middle row: B_g. Bottom row: A_u and B_u. Calculated frequencies in cm^{-1} shown.

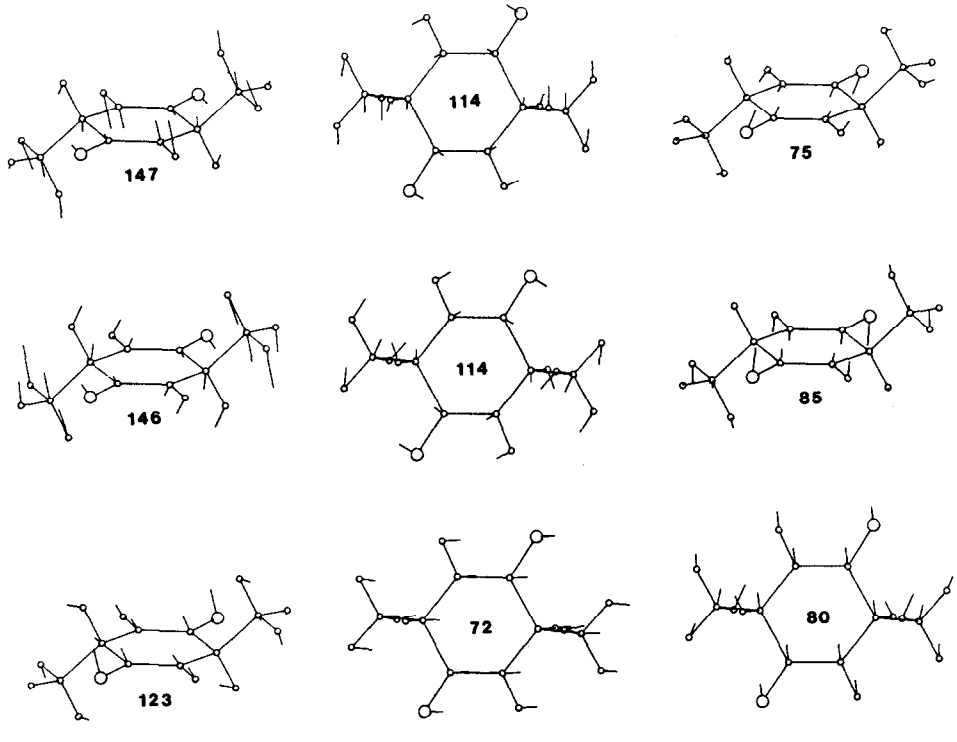

Fig. 17. Lattice modes of form II. Oxygen atoms drawn extra large. Top row: A_g. Middle row: B_g. Bottom row: A_u and B_u. Calculated frequencies in cm^{-1} shown.

Figures 16 and 17 show the calculated atomic displacements for the lattice modes. For the z librations, about the normal to the ring, the calculated splitting between the in-phase (A_g) and out-of-phase (B_g) modes in both **I** and **II** is too small, with the A_g frequency too high. The A_g mode is expected to be more anharmonic than the B_g because the diagonal cubic term of the potential energy in the normal coordinates vanishes for all except the totally symmetric species. This term would cause a lowering of the A_g frequency. We have found a similar increase in splitting due to a difference in diagonal cubic anharmonicity between the symmetric and antisymmetric C=O str modes in the formic acid dimer [20]. Finally we note that the calculated frequencies are not especially sensitive to the H · · · O force constant. When we set this force constant to zero, the largest shift is for the B_u mode in **I**, which decreases by only 14 cm^{-1}, while the other modes shift by less than 10 cm^{-1}. Thus, unfortunately, our data cannot be used to determine a more reliable value for the H · · · O interaction.

We conclude our discussion of the spectral assignments with some general remarks. Except for the CO ob mode, the peptide group frequencies, particularly in **II**, agree well with those found in cyclo(Gly-Gly), with differences that can be related to structural differences. We have not made detailed comparisons of calculated and observed frequencies because we have not refined the force constants transferred from cyclo(Gly-Gly) and alkanes. Nevertheless, Table 2 shows that the agreement is fairly good for most of the modes. The major discrepancies are for the Raman CO str, the i.r. CN str, and the CO ob and ring tor modes. The CO ob requires new interactions that were not important in cyclo(Gly-Gly), and the torsional force constants for cyclo(Gly-Gly) were less reliably determined because of the sensitivity of the ring tor modes to the intermolecular potential. We should mention that, within the framework of the present unrefined force field, the alkane force constants proved to be more satisfactory, especially in the 900–1400 cm^{-1} region, than the poly (L-alanine) force fields [21, 22] for the $C^{\alpha}H^{\alpha}$ ($C^{\beta}H_3$) group. In conclusion, the present set of force constants is a good starting point for refinement of a force field for cyclo(D-Ala-L-Ala).

EFFECT OF HYDROGEN BOND STRUCTURE ON PEPTIDE GROUP MODES

We have seen above that there are differences in the bands due to the CONH group in **I** and **II**. In trying to understand these differences, we first note that since both CO and NH groups participate in hydrogen bonds, these modes are likely to be sensitive to the hydrogen bond strength, and that there will be strong intermolecular interactions between peptide groups hydrogen bonded to each other. We next note that the essential structural differences in **I** and **II** are in the hydrogen bond pattern and in the strength of each hydrogen bond. That is, in **I** the crystal packing is such that each CONH group hydrogen bonds to other groups related to it by a two-fold screw operation, whereas in **II** the hydrogen bonds are formed between CONH groups related by the inversion operation. We therefore expect that the factor group splittings of the peptide group modes will tend to be such that in **I** a large A–B splitting will be seen whereas in **II** a large g–u splitting will be observed. As we have noted earlier, the dimensions (Fig. 1) of each NH · · · OC group in **I** and **II** indicate that the hydrogen bond in **II** is stronger than in **I**. That is, the shorter N · · · O distance, the longer C=O bond, the more nearly linear NH · · · O angle, and a CO · · · N angle closer to 120° all are indicative of a stronger interaction as measured, in particular, by frequency shifts [6]. This difference in hydrogen bond strength would be reflected in a shift between **I** and **II** in the average frequency, over factor group components, of each peptide group mode.

We now discuss to what extent these considerations are borne out for each of the modes of the CONH group. Except in one instance, we will not attempt here quantitative explanations of the observations.

The mode showing the most striking differences between **I** and **II** is the NH str. Of these differences, the roughly 100 cm^{-1} downward shift of the ND str band (and an estimated 140 cm^{-1} decrease in the NH str frequency) from **I** to **II** is most readily explained as being due to a stronger hydrogen bond in **II**. By taking a model system of *N*-methylacetamide hydrogen bonded to a formamide molecule, with N · · · O distance and HNO and CON angles as in **I** and **II**, respectively, we can use the method described previously [6] to compute the harmonic force constant of the NH str mode. The frequency shift from **I** to **II** given by the scaled STO–3G force constants is 89 cm^{-1} for the NH str mode and 65 cm^{-1} for the ND str. Thus, the observed difference in frequency is qualitatively corroborated by *ab initio* calculations on a model system. Looking at the hydrogen bond dimensions in **I** and **II**, we see that while the N · · · O distance in **I** is only 0.007 Å longer than in **II**, which by itself would lead to a calculated shift of less than 2 cm^{-1} [6], the HNO and CON angles in **I** are significantly less favorable. That such differences in the angles can result in a frequency shift of over 100 cm^{-1} in the NH str mode shows the importance of considering the HNO and CON angles as well as the N · · · O distance in estimating the strength of a hydrogen bond. This strong dependence of the NH str frequency on the angles also implies that one should not expect to find a correlation of NH str frequency with the N · · · O distance. As we have suggested [6], that such a correlation does seem to be observed [23] may be the result of an approximate correlation of NHO angles with N · · · O distance [24, 25]. A similar explanation probably applies to other types of hydrogen bonds.

We next consider the differences in the fine structure and width of the NH str mode. An understanding of these differences may be gained by looking at oxalic acid, another molecule that crystallizes in two forms: α-

oxalic acid with chains formed by OH · · · O hydrogen bonds between molecules related by two-fold screw symmetry, and β-oxalic acid with centrosymmetric hydrogen bonded rings [26, 27]; the dimensions indicate a stronger hydrogen bond in β. The i.r. spectra of the OH str mode in α and β [28] resemble closely the NH str bands in I and II respectively. WITKOWSKI and WÓJCIK [29] have managed to reproduce remarkably well the width and fine structure in both α and β, as well as the marked narrowing on deuteration, using a quantitative theory of hydrogen bond spectra [30]. In this theory, for an isolated X–H · · · Y hydrogen bond, anharmonic coupling of the XH str mode with the low frequency X · · · Y str mode results in a Franck–Condon progression due to simultaneous excitations of the high and low frequency modes; the spacing between adjacent transitions is determined by the low frequency mode. In crystals, resonant interaction, for example dipole–dipole coupling, between nearby XH groups causes factor group splittings which further spread out the XH str band and destroy the regularity of the sub-band positions. Further complications are caused by Fermi resonance with overtones and combinations [31]. The difference in complexity in the two forms of oxalic acid arises if one assumes in β a stronger anharmonic coupling because of the stronger hydrogen bond and a stronger resonant interaction because of the closeness of the OH groups in a cyclic ring.

We may expect that a similar explanation applies to cyclo(D-Ala-L-Ala). We have already discussed the stronger hydrogen bond in II, which would lead to a stronger anharmonic coupling with low frequency modes. A theoretical basis for this coupling has been provided by our recent *ab initio* study [6], which shows large changes in the NH str force constant as the N · · · O distance and HNO and CON angles are varied. Lattice modes that involve displacements of these intermolecular coordinates would therefore be expected to be strongly coupled to the NH str mode. It is tempting to infer from the approximate 40 cm^{-1} spacing of the i.r. sub-band positions in I the frequency of the lattice mode involved. However, we must also consider the *A–B* splitting, measured to be about 19 cm^{-1} in the Raman, and the possibility of coupling with more than one lattice mode.

In polypeptides and polyamides with *trans* peptide units, the narrower and apparently singlet nature of the NH str band may be attributed to the weaker hydrogen bonds, as evidenced by the frequency of about 3250–3300 cm^{-1}, and the smaller resonant interactions between peptide groups that are farther apart than is possible in *cis* peptides. Nevertheless, the possibility remains that there is unresolved fine structure in the NH str band of polypeptides [17]. We may also conclude that in *cis* peptides and in amides, a broad, complex NH str band is indicative of a cyclic hydrogen bonded structure.

We conclude our discussion of the NH str mode by mentioning the usefulness of cyclo(D-Ala-L-Ala) and cyclo(Gly-Gly) as models for testing the WITKOWSKI–MARÉCHAL theory in the case of peptide structures. In I and II we see the effects of different resonant interactions and different hydrogen bond strengths; and in II and cyclo(Gly-Gly) the hydrogen bond geometries are very similar but the low frequency modes are different. In all three structures, our large amount of data and the relatively high symmetry should facilitate analysis, particularly of possible Fermi resonance interactions. And finally, quantitative estimates of the anharmonic coupling parameters may be derived from our study of the variation of the NH str force constant with hydrogen bond geometry [6].

We turn now to the other peptide group modes, all of which show considerably smaller differences between I and II than does the NH str. Table 4 summarizes our results on these modes; where *A–B* splittings are observed the average frequencies are given, with the splitting in parentheses. Also shown for some modes are the averages over the Raman and i.r. frequencies and the *g–u* splitting.

Looking at the NH ib mode, we see in I a sizable (40 cm^{-1}) *g–u* splitting. Much of this is probably a result of intramolecular coupling between the peptide units in each molecule and reflects the relatively delocalized nature of the NH ib mode. Indeed, in II the larger *g–u* splitting may be ascribed to the additional intermolecular interaction between peptide units in the hydrogen bonded ring. The shift of the mean *g–u* frequency from 1415 cm^{-1} in I to 1458 cm^{-1} in II is a measure of the increase in strength of the hydrogen bond; the change represents a 3% increase, compared with the approximately 4.3% decrease of the NH str frequency from I to II. The ND ib mode is a highly mixed mode and is not expected to show clear trends indicative of the hydrogen bonding.

The well-localized NH ob mode shows clearly the effects of structural differences. The Raman mode in I has a 21 cm^{-1} *A–B* splitting whereas that in II has none. The i.r. mode in I may have a splitting of about 16 cm^{-1} if we assign a sharp, distinct band resolved in the low temperature spectrum to the other factor group component. The *g–u* splitting of 4 cm^{-1} in I increases to 27 cm^{-1} in II, where the mean *g–u* frequency shifts up by 4.5%. Thus, the NH ob is relatively as sensitive to hydrogen bond strength as the NH str, a point emphasized by BANDEKAR and ZUNDEL [32] on the basis of temperature studies of uracil.

Next to the NH str, the CO str mode shows the most interesting differences between I and II. To help understand the changes in this mode, we have to note that it has a large contribution from NH ib. This intramolecular interaction is evidenced by the 19 cm^{-1} shift from H_2O to D_2O solution. Furthermore, in the solid materials, the Raman intensity increases in the ND compounds where the mode is more purely CO str, and on deuteration the mean *g–u* frequency decreases by 19 cm^{-1} in I and by 30 cm^{-1} in II; the larger magnitudes of these intensity and frequency

Table 4. Summary of observed frequencies (in cm^{-1}) of peptide group vibrations in cyclo(D-Ala-L-Ala)*

	I	II	I–ND	II–ND	H_2O	D_2O
NH/ND *in-plane bend*						
Raman	1395	1428	1245	1244	1404	1228
i.r.	1435	1488	1225	1234		
g–u	1415(40)	1458(60)				
NH/ND *out-of-plane bend*						
Raman	804(21)	826	568(13)	591		
i.r.	808	853	593	616		
g–u	806(4)	840(27)				
CO *stretch*						
Raman	1654(48)	1658(20)	1637(42)	1618(13)	1664	1645
i.r.	1664(25)	1674(27)	1643(25)	1654(21)		1643
g–u	1659(10)	1666(16)	1640(6)	1636(36)		1644(2)
CO *in-plane bend*						
Raman	612	616	599	606	610	597
i.r.	433(9)	453(4)	421(12)	445(8)		
CO *out-of-plane bend*						
Raman	672	661	683	663	662	668
i.r.	698	692	719	704		
CN *stretch*						
Raman	1523	1516	1495	1490	1517	1500
i.r.	1468	1470	1459	1467	1475	1466

*Observed splittings in parentheses. Rows labelled "*g–u*" are averages of Raman and i.r. frequencies with *g–u* splitting in parentheses.

changes in **II** are because of the higher amount of NH ib contribution as a result of the higher NH ib frequency, which in turn arises from the stronger hydrogen bond in **II**. With this NH ib mixing in mind, then, we observe that in the NH crystals the mean *g–u* frequency shifts up by 7 cm^{-1} from **I** to **II**, whereas it shifts down by 4 cm^{-1} in the ND compounds. The explanation is that while a pure CO str mode would decrease in frequency as the hydrogen bond strength increases, a high NH ib contribution causes the net shift to be upward. We see from the 4 cm^{-1} shift in the ND compounds that the CO str mode is only slightly sensitive to hydrogen bond strength. On the other hand, the changes in hydrogen bond pattern have significant effects, particularly in the ND compounds, where the *g–u* splitting is much larger in **II** but where the *A–B* splitting is larger in **I**. This trend is also present in the NH crystals but to a lesser degree for the *g–u* splitting. The i.r. *A–B* splittings are not as clear-cut as the Raman splittings, and probably depend on the details of the intermolecular interaction. Thus, as for the NH ob, the extensive data on the CO str mode confirm very nicely the pattern of splittings expected. Quantitative calculations of the splittings are planned using electrostatic interaction models, in particular dipole–dipole coupling [33] and Coulombic interactions between dynamical atomic partial charges, i.e. atomic charges that are allowed to vary in magnitude as well as position during vibrational motion [20]. We note that representations of van der Waals interactions such as the atom–atom 6–12 potential fail to give any significant splitting of the CO str mode.

The i.r. CO ib mode shifts up by 4.6% from **I** to **II** and shows a larger *A–B* splitting in **I**. The low frequency of this mode and its mixing with skeletal and side-chain motions probably make it sensitive to other non-bonded interactions as well. The CO ob is also strongly mixed and is not expected to show trends indicative of hydrogen-bond interactions.

The CN (or $C^{\alpha}CN$) str mode does not show any meaningful trends: the Raman mode decreases from **I** to **II** but the i.r. mode increases. In any case, it does not seem particularly sensitive to hydrogen bonding. This implies that the *trans* amide **II** and **III** modes, which involve CN str and NH ib, owe their sensitivity to hydrogen bonding primarily to the NH ib component.

In summary, of the peptide group modes, the three stretching and bending modes of the NH bond are extremely sensitive to the hydrogen bond strength, whereas those of the CO bond are much less so.

EFFECT OF STRUCTURE ON CH MODES

Table 5 summarizes the Raman frequencies of the CH_3 and CH^{α} stretch and H^{α} bend modes in **I** and **II**, together with the values for crystalline L-alanine [14]. We see that while the lower frequency CH_3 as mode remains constant, the higher frequency CH_3 as increases from **I** to **II**. On the other hand, the higher frequency H^{α} b decreases from L-alanine to **I** to **II**, as does the CH^{α} str. Also observed, but not listed, is a 20 cm^{-1} shift of one of the i.r. CH_3 rock modes from I–ND to **II**–ND.

Table 5. Correlation of Raman $C^{\beta}H_3$ and $C^{\alpha}H^{\alpha}$ frequencies with structure

		L-Ala	I	II
Observed frequencies (in cm^{-1})				
CH_3 antisymmetric stretches		3001	2998	3011
		2987	2984	2985
splitting		14	14	26
CH^{α} stretch		2968	2914	2893
H^{α} bends		1359	1323	1313
		1305	1303	1300
splitting		54	20	13
Structural parameters				
	$C^{\beta}C^{\alpha}H^{\alpha}$	110.4°	108.2°	109.5°
Angle from	CH^{α}	57.9	56.8	59.2
$NC^{\alpha}C$ plane	$C^{\alpha}C^{\beta}$	52.5	51.4	50.2
Dihedral	$OCC^{\alpha}H^{\alpha}$	44.8	59.7	64.6
angles	$OCC^{\alpha}C^{\beta}$	−76.8	−57.8	−53.1
(L-residue)				
	$C^{\alpha}C^{\beta}H$	110.3	107.6	109.6
		110.6	110.3	109.8
		110.4	112.4	108.2
	$H^{\beta}C^{\beta}H^{\beta'}$	108.9	115.2	108.3
		108.4	107.8	110.2
		108.2	102.9	110.7
	$H^{\beta}C^{\beta}C^{\alpha}H^{\alpha}$	175.2	−176.4	−174.6
Dihedral		55.5	66.3	64.2
angles		−65.1	−63.7	−53.8

As we have seen, the persistence of the differences in the H^{α} b and CH_3 rock modes in solution shows that these changes are due to intramolecular effects. Indeed, we can rule out the possibility that the decrease in the CH^{α} str frequency in **II** is due to formation of an intermolecular $CH^{\alpha} \cdots O$ hydrogen bond: the nearest $H^{\alpha} \cdots O$ contacts in **I** and **II** are 2.41 and 2.67 Å, respectively, with similarly unfavorable $CH^{\alpha} \cdots O$ angles of about 156° in both. Fermi resonance effects are also not likely because, of the CH str modes, only the CH_3 ss shows evidence in the polarized spectra of being perturbed.

If we then look at the results of normal mode calculations on isolated molecules of **I**- and **II**-type conformations, using the same force field and with all CH bond lengths set to 1.09 Å, we find trends inconsistent with what are observed: the CH_3 as splitting decreases from **I** to **II**, the H^{α} b splitting increases from **I** to **II** in the Raman and decreases in the i.r., and the CH^{α} str is unchanged in **I** and **II**. To get shifts of these modes in the correct directions, therefore, it is necessary to allow different force constants and probably also different CH bond lengths in the two molecules. Unfortunately, the X-ray determinations [3–5] cannot tell us whether the CH bond lengths are different because X-ray CH bond lengths are highly unreliable [34]. We therefore have to resort to *ab initio* calculations.

The CH^{α} bond length and stretching force constant are most easily obtained. We used the STO-3G basis and the procedure described in [6]: keeping the other internal coordinates at their experimental values, we optimized the CH^{α} bond and then derived the diagonal force constant from the analytical energy gradient. The CH^{α} str mode is localized, and this procedure is adequate; for the other modes, more extensive optimizations are needed followed by determination of off-diagonal as well as diagonal force constants. We mention first that the SCF energy of conformation **II** was found to be 3.4 kcal/mole lower than that of **I**, which is consistent with the observation that **II** predominates in solution. (We recall, however, that the crystalline form **I** is slightly favored according to our crystal-packing calculations.) The equilibrium CH^{α} bond lengths indeed turn out to be different, 1.0973 Å (**I**) and 1.0984 Å (**II**), and the diagonal stretching force constants are 7.055 mdyne/Å (**I**) and 7.000 mdyne/Å (**II**). Using the Jacobian matrix element $\Delta\nu/\Delta f$ of 312 cm^{-1}/(mdyne/Å), we get a decrease in the CH^{α} str frequency from **I** to **II** of 17 cm^{-1}. Our result of a frequency change of 17 cm^{-1} for a 1.1×10^{-3} Å change in CH^{α} bond length compares well with the value of 16 cm^{-1} per 10^{-3} Å for deuterium-isolated CH bonds in *n*-alkanes found by AJILBURY *et al.* [35] using higher-level *ab initio* calculations. A scaling factor of 4.6/7.0 for our *ab initio* force constants must be applied, a value of 4.6 mdyne/Å being needed to fit the observed frequency of 2893 cm^{-1} in **II**; we then get a shift of 11 cm^{-1}. Although this is only half the 21 cm^{-1} observed shift, we can conclude that the shift is due to a difference in the CH^{α} force constant in the two conformations. In support of this, the X-ray data show the more nearly axial $C^{\alpha}C^{\beta}$ bond in **I** to be longer than the more nearly equatorial $C^{\alpha}C^{\beta}$ bond in **II**, 1.525 Å versus 1.518 Å [3, 5]. Since the CH^{α} bond in **I** is more nearly equatorial, it may be expected to be

shorter than in **II** and therefore to have a higher force constant.

It may well be that the difference in the CH^{α} bond is a result of the total intramolecular environment. Nevertheless, it is useful to look for one or a few structural parameters that might be primarily responsible, as indicated by trends similar to those for the CH^{α} str and H^{α} b frequencies. We have listed in Table 5 some parameters involving the CH^{α} and $C^{\alpha}C^{\beta}$ bonds for **I** and **II**, and also for L-alanine [36] on the assumption that the charged groups do not introduce significant additional effects. We note first that intramolecular $CH^{\alpha} \cdots O$ hydrogen bonding is ruled out in view of the $H^{\alpha} \cdots O$ distances: 2.65 Å (**I**) and 2.63 Å (**II**). The $C^{\beta}C^{\alpha}H^{\alpha}$ angle also does not seem a likely candidate. The angle of the CH^{α} bond from the $NC^{\alpha}C$ plane shows a 2.4° change from **I** to **II**, but the value for L-alanine does not fit the trend. The dihedral angle $OCC^{\alpha}H^{\alpha}$ seems promising, with a correct trend and a larger difference between L-alanine and **I** than between **I** and **II**. (The variation in the $NCC^{\alpha}H^{\alpha}$ angle is similar because of planarity at the sp^2 carbon.) Accordingly, we computed with the STO-3G basis the CH^{α} bond length and force constant in a model system in which the comparable dihedral angle was varied, viz. a linear all-*trans* blocked alanine (CH_3–NH–$C^{\alpha}H^{\alpha}C^{\beta}H_3$–C′O–$C_1H_3$) with $C_1C'C^{\alpha}H^{\alpha}$ and $C_1C'C^{\alpha}C^{\beta}$ angles equal to the $OCC^{\alpha}H^{\alpha}$ and $OCC^{\alpha}C^{\beta}$ angles in L-alanine, **I** and **II**, respectively. The scaled force constants give shifts of 42 cm^{-1} from L-alanine to **I**, and 23 cm^{-1} from **I** to **II**, compared to the observed shifts of 54 and 21 cm^{-1}, respectively. The bond length increases by 2.1×10^{-3} Å from **I** to **II**, giving a shift of 10 cm^{-1} per 10^{-3} Å bond-length change. Thus, there is a significant variation in the CH^{α} bond length and force constant with the adjacent dihedral angle.

Our findings on the CH^{α} bond are consistent with spectroscopic and *ab initio* studies of CH bonds in hydrocarbons and other molecules [35, 37, 38]. For deuterium-isolated CH groups in cyclohexane, the equatorial CH str mode is about 30 cm^{-1} higher than the axial CH str mode [39–41]. *Ab initio* calculations confirm that the equatorial CH bond is shorter by 1.7×10^{-3} Å [35, 42]. Variations in the CH bond lengths of a methyl group have also been found, an in-plane CH bond being shorter than the out-of-plane bonds [35, 37, 38]. Finally, calculations on several conformers of *N*-acetyl-*N*′-methyl alanyl amide show significant changes in the CH^{α} bond length (as well as in other parameters) [43]. Our present work extends to peptides these studies on the sensitivity of CH bonds to molecular environment, providing definitive results on conformations for which X-ray data are available, and also shows the possibility of similar studies of the CH bend modes. The conformational dependence of the CH^{α} modes is potentially very useful in studying structure in peptides and polypeptides. If it is difficult to assign the CH^{α} str mode, the CD^{α} str may be used.

Turning to the CH_3 modes, we find it more difficult to identify a structural parameter that correlates well with the frequencies. According to the angles involving the $C^{\beta}H$ bonds, the CH_3 group in **I** seems the most asymmetric, yet the splitting of the CH_3 as modes is smaller than in **II**. The higher degree of asymmetry of the CH_3 group in **I**, resulting in different kinetic couplings between the $C^{\beta}H$ bonds, probably explains why our normal mode calculations using a single set of force constants give a larger splitting in **I** than in **II**. At the same time it is also likely that the individual $C^{\beta}H$ bonds are different in length and have different diagonal and interaction force constants. Although a neutron diffraction study of L-alanine [36] shows identical $C^{\beta}H$ bond lengths, to within experimental error, spectroscopic and *ab initio* studies, as mentioned above, have found different CH bond lengths in methyl groups in various molecules, including L-alanine [44]; in *N*-acetyl-*N*′-methyl alanyl amide, in addition, the $C^{\beta}H$ bonds were found to vary with conformation [43]. Preliminary *ab initio* calculations, with limited optimizations, of **I** and **II** also indicate different $C^{\beta}H$ bond lengths, both within each conformation and between the two conformers. Thus, the differences in the CH_3 modes in **I** and **II** probably arise from differences in both the *G* and *F* matrix elements.

CONCLUSIONS

We have followed up our previous study of cyclo(Gly-Gly) [1, 2] with a detailed vibrational analysis of cyclo(D-Ala-L-Ala). Our results provide a better understanding of the modes of the *cis* CONH group in peptides with larger side chains, and complement the large body of work on the *trans* amide group in peptides and polypeptides [45].

That cyclo(D-Ala-L-Ala) crystallizes in two forms, for which X-ray data are available, presents a rare opportunity to study experimentally the sensitivity of the peptide group modes to hydrogen bonding. Our extensive data have allowed us to correlate the differences in these modes in the two forms with the different hydrogen bond patterns and strengths. Quite unexpectedly, we have also found differences in the CH modes and have attributed these to the different molecular conformations, a conclusion supported by *ab initio* calculations on the CH^{α} stretch mode. In view of the potential importance of a frequency–structure correlation of the CH modes, further *ab initio* and experimental work to examine the precise nature of this correlation would be useful.

The significant spectral differences in the two forms imply that it will not be possible to refine a single intramolecular valence force field for both structures. Rather, we think that a more fruitful approach is to develop a molecular mechanics force field [46] that will yield simultaneously both molecular structures as well as the shifts in the peptide group and CH modes. Such an empirical energy function might incorporate the

atom–atom potential of MOMANY *et al.* [12], which we have shown to be very effective in lattice dynamical calculations.

Acknowledgement—This research was supported by National Science Foundation grants DMB-8517812 and DMR-8303610. We are indebted to Prof. K. D. KOPPLE for providing the sample of cyclo(D-Ala-L-Ala).

REFERENCES

[1] T. C. CHEAM and S. KRIMM, *Spectrochim. Acta* **40A**, 481 (1984).
[2] T. C. CHEAM and S. KRIMM, *Spectrochim. Acta* **40A**, 503 (1984).
[3] J. SLETTEN, *Acta Chem. Scand.* **A34**, 593 (1980). (The z-coordinate of oxygen in Table 1 of this reference should read 0.0029(1).)
[4] E. BENEDETTI, P. CORRADINI and C. PEDONE, *J. phys. Chem.* **73**, 2891 (1969).
[5] E. SLETTEN, *J. Am. chem. Soc.* **92**, 172 (1970).
[6] T. C. CHEAM and S. KRIMM, *J. molec. Struct.* **146**, 175 (1986).
[7] H. BROCKMANN and H. MUSSO, *Chem. Ber.* **89**, part 2, 241 (1956).
[8] P. STEIN, Ph.D. Thesis, University of Oregon (1973).
[9] M. KOBAYASHI, *J. chem. Phys.* **70**, 4797 (1979).
[10] W. H. MOORE and S. KRIMM, *Biopolymers* **15**, 2465 (1976).
[11] R. G. SNYDER and J. H. SCHACHTSCHNEIDER, *Spectrochim. Acta* **21**, 169 (1965).
[12] F. A. MOMANY, L. M. CARRUTHERS, R. F. MCGUIRE and H. A. SCHERAGA, *J. phys. Chem.* **78**, 1595 (1974).
[13] D. M. BYLER and H. SUSI, *Spectrochim. Acta* **35A**, 1365 (1979).
[14] H. SUSI and D. M. BYLER, *J. molec. Struct.* **63**, 1 (1980).
[15] M. DIEM, P. L. POLAVARAPU, M. OBOODI and L. A. NAFIE, *J. Am. chem. Soc.* **104**, 3329 (1982).
[16] R. DEGEILH and R. E. MARSH, *Acta crystallogr.* **12**, 1007 (1959).
[17] A. ELLIOTT, *Proc. R. Soc.* **A226**, 408 (1954).
[18] H. BOUTIN and S. YIP, *Molecular Spectroscopy with Neutrons*, p. 202. MIT Press, Cambridge (1968).
[19] A. WARSHEL, *Comput. Chem.* **1**, 195 (1977).
[20] J. DYBAL, T. C. CHEAM and S. KRIMM, *J. molec. Struct.*, **159**, 183 (1987).
[21] J. F. RABOLT, W. H. MOORE and S. KRIMM, *Macromolecules* **10**, 1065 (1977).
[22] A. M. DWIVEDI and S. KRIMM, *Macromolecules* **15**, 186 (1982); *ibid.* **16**, 340 (1983).
[23] A. LAUTIÉ, F. FROMENT and A. NOVAK, *Spectrosc. Lett.* **9**, 289 (1976).
[24] R. TAYLOR and O. KENNARD, *Acc. Chem. Res.* **17**, 320 (1984).
[25] E. N. BAKER and R. E. HUBBARD, *Prog. Biophys. molec. Biol.* **44**, 97 (1984).
[26] S. B. HENDRICKS, *Z. Krist.* **91**, 48 (1935).
[27] E. G. COX, M. W. DOUGILL and G. A. JEFFREY, *J. Chem. Soc.*, 4854 (1952).
[28] L. J. BELLAMY and R. J. PACE, *Spectrochim. Acta* **19**, 435 (1963).
[29] A. WITKOWSKI and M. WÓJCIK, *Chem. Phys.* **21**, 385 (1977).
[30] Y. MARÉCHAL and A. WITKOWSKI, *J. chem. Phys.* **48**, 3697 (1968).
[31] M. WÓJCIK, *Molec. Phys.* **36**, 1757 (1978).
[32] J. BANDEKAR and G. ZUNDEL, *Spectrochim. Acta* **38A**, 815 (1982).
[33] T. C. CHEAM and S. KRIMM, *Chem. Phys. Lett.* **107**, 613 (1984).
[34] W. C. HAMILTON and J. A. IBERS, *Hydrogen Bonding in Solids*. Benjamin, New York (1968).
[35] A. L. AJILBURY, R. G. SNYDER, H. L. STRAUSS and K. RAGHAVACHARI, *J. chem. Phys.* **84**, 6872 (1986).
[36] M. S. LEHMANN, T. F. KOETZLE and W. C. HAMILTON, *J. Am. chem. Soc.* **94**, 2657 (1972).
[37] D. C. MCKEAN, J. E. BOGGS and L. SCHÄFER, *J. molec. Struct.* **116**, 313 (1984).
[38] L. SCHÄFER, J. D. EWBANK, V. J. KLIMKOWSKI, K. SIAM and C. VAN ALSENOY, *J. molec. Struct. (Theochem.)* **135**, 141 (1986).
[39] J. CAILLOD, O. SAUR and J.-C. LAVALLEY, *Spectrochim. Acta* **36A**, 185 (1980).
[40] J. S. WONG, R. A. MACPHAIL, C. B. MOORE and H. L. STRAUSS, *J. phys. Chem.* **86**, 1478 (1982).
[41] R. G. SNYDER, A. L. AJILBURY, H. L. STRAUSS, H. L. CASAL, K. M. GOUGH and W. F. MURPHY, *J. chem. Phys.* **81**, 5352 (1984).
[42] N. S. CHIU, J. D. EWBANK and L. SCHÄFER, *J. molec. Struct.* **86**, 397 (1982).
[43] J. N. SCARSDALE, C. VAN ALSENOY, V. J. KLIMKOWSKI, L. SCHÄFER and F. A. MOMANY, *J. Am. chem. Soc.* **105**, 3438 (1983).
[44] H. SELLERS and L. SCHÄFER, *Chem. Phys. Lett.* **63**, 609 (1979).
[45] S. KRIMM and J. BANDEKAR, *Adv. Protein Chem.* **38**, 181 (1986).
[46] U. BERKERT and N. L. ALLINGER, *Molecular Mechanics*. American Chemical Society, Washington D.C. (1982).